

Modeling study of the impact of SO₂ volcanic passive emissions on the tropospheric sulfur budget

Claire Lamotte¹, Jonathan Guth¹, Virginie Marécal¹, Martin Cussac¹, Paul David Hamer², Nicolas Theys³, and Philipp Schneider²

¹CNRM, Université de Toulouse, Météo-France, CNRS, Toulouse, France

²NILU – Norwegian Institute for Air Research, P.O. Box 100, 2027 Kjeller, Norway

³Royal Belgian Institute for Space Aeronomy, BIRA-IASB, Brussels, Belgium

Correspondence: Lamotte Claire (claire.lamotte@meteo.fr)

Abstract. Well constraining volcanic emissions inventories in chemistry-transport models is necessary to study the impacts induced by these sources on the tropospheric sulfur composition, as well as on sulfur species concentrations and depositions at the surface. In this paper, the changes induced by the update of the volcanic sulfur emissions inventory are studied using the global chemistry-transport model MOCAGE (MODèle de Chimie Atmosphérique à Grande Échelle). Unlike the previous inventory [Andres and Kasgnoc (1998)], the updated one [Carn et al. (2016, 2017)] uses more accurate information and includes contributions from both passive degassing and eruptive emissions. Eruptions are provided as daily total amounts of sulfur dioxide (SO₂) emitted by volcanoes in the [Carn et al. (2016, 2017)] inventories, and degassing emissions are provided as annual averages with the related mean annual uncertainties of those emissions by volcano. Information on plumes altitudes is also available and has been used in the model. We choose to analyse the year 2013, for which only a negligible amount of eruptive volcanic SO₂ emission is reported, allowing us to focus the study on the impact of passive degassing emissions on the tropospheric sulfur budget. An evaluation against OMI SO₂ total column and MODIS AOD observations shows the improvements of the model results with the updated inventory. Because the global volcanic SO₂ flux changes from 13 Tg yr⁻¹ in [Andres and Kasgnoc (1998)] to 23.6 Tg yr⁻¹ in [Carn et al. (2016, 2017)], significant differences appears in the global sulfur budget, mainly in the free troposphere and in the tropics. Even though volcanic SO₂ emissions represent 15 % of the total annual sulfur emissions, the volcanic contribution to the tropospheric sulfate aerosol burden is 27 %, which is due to the higher altitude of emissions from volcanoes. Moreover, a sensitivity study on passive degassing emissions, using the annual uncertainties of emissions per volcano, also confirmed the non-linear link between tropospheric sulfur species content with respect to volcanic SO₂ emissions. This study highlights the need for accurate estimates of volcanic sources in chemistry-transport models in order to properly simulate tropospheric sulfur species.

20 1 Introduction

Sulfur emissions come mainly from human activities (fossil fuel combustion) and volcanic activity [Andreae (1985)]. Among them, sulfur dioxide (SO₂) is a pollutant species, known to affect both human health and the environment. Because of their link to the formation of acid rain and sulfate aerosols which can induce climate forcing [Chestnut (1995), Robock (2000, 2007),

Smith et al. (2001), Schmidt et al. (2012), Kremser et al. (2016)], SO₂ emissions became a major concern in environmental policies. In some regions of the world, these policies led to strong reductions in anthropogenic SO₂ emissions in recent decades [Fioletov et al. (2016), Krotkov et al. (2016), Aas et al. (2019)]. Over North America and Europe, emissions strongly decreased between 2005 and 2015. In the East Asian region, the decrease only happened after 2010 [Sun et al. (2018)]. In contrast, over India, emissions strongly increased. And over other large SO₂-emitting regions (Mexico, South Africa, Russia or Middle East), they remained stable since 2000. However, the decrease in anthropogenic SO₂ emissions over Europe and North America was sufficient to induce an overall decrease at the global scale. Moreover, Graf et al. (1997) concluded that the efficiency of volcanic emissions to contribute to the tropospheric sulfate burden is greater than the efficiency of anthropogenic emissions, mostly because SO₂ lifetime increases with altitude and therefore has an impact for longer time periods and over larger areas. This means that in the regions where anthropogenic sulfur emissions have decreased, and more generally at the global scale, the relative proportion of volcanic sulfur emissions against the total sulfur emissions has increased.

In order to better understand the processes leading to variations in the sulfur species budget, the role of modelling is important. At the global scale, emission inventories (compilation of all available data on the globe) are used in models. Until recently, the most effective measurement instruments to assess volcanic emissions for building the inventories were the CO₂-correlation SPECTrometer (COSPEC) ground-based instruments [details in Sect. 3.1, Moffat and Millan (1971), Williams-Jones et al. (2008)] or one of the first satellite instruments (such as the Total Ozone Mapping Spectrometer, TOMS) [Krueger et al. (1995), Seftor et al. (1997), Torres et al. (1998a, b)] but which provides only crude measurements of SO₂ column. Andres and Kasgnoc (1998) used these instruments to create one of the first global inventories of volcanic sulfur emissions. Furthermore, being compiled for the Global Emissions Inventory Activity (GEIA), it is the most widely used global dataset. For example, it has been implemented in several climate and chemistry-transport models [Chin et al. (2000), Liu et al. (2005), Shaffrey et al. (2009), Emmons et al. (2010), Lamarque et al. (2012), Savage et al. (2013), Walters et al. (2014), Michou et al. (2015)] and used in various studies on climate aerosol radiative forcing, ocean dimethyl sulfide (DMS) sensitivity or tropospheric aerosol budget [Adams et al. (2001), Takemura (2012), Michou et al. (2019), Gondwe et al. (2003a, b), Gunson et al. (2006), Liu et al. (2007)]. Subsequently, other studies using similar techniques, or building on this first inventory by supplementing it with documented sets of sporadic eruptions, have provided further global inventories [Halmer et al. (2002), Diehl et al. (2012)].

But at the time these inventories were built, techniques for measuring emission fluxes were not very accurate for the determination of volcanic sources. Indeed, ground-based instruments can only be deployed at easy-to-access volcanoes (and there are few such as, *e.g.*, Masaya) and TOMS detection sensitivity was limited only to the largest eruptions. The available inventories were therefore incomplete. The study of Andres and Kasgnoc (1998), with only one average value of all 25 years data measurements collected per volcano, reflects only a climatology without time variability. However, a lot of improvements have been made recently on satellite technologies, making possible to monitor volcanic emissions more accurately. The satellite global coverage enables to detect emission fluxes even from hard-to-access volcanoes. The improved sensitivity of the measurements has also made possible to detect not only the largest eruption fluxes but also smaller ones and persistent degassing [Yang et al. (2010), Thomas et al. (2011), Carn et al. (2013), Li et al. (2013)]. Thanks to newly developed algorithms, information on injection altitudes is available [Yang et al. (2009, 2010, 2013), Nowlan et al. (2011), Rix et al. (2012), Clarisse et al. (2014)],

reducing the uncertainties of the characterization of volcanic sources. Ge et al. (2016) highlighted the improvements made on the sulfate direct radiative forcing using both eruptive and passive degassing data in a chemistry-transport model and stressed the importance of considering the SO₂ injection altitude in volcanic emission inventories.

Carn et al. (2016, 2017) sought to compile all those new higher quality data, compared to Andres and Kasgnoc (1998), in order to provide a more representative inventory of volcanic SO₂ emissions. It is a compilation of both eruptions and passive degassing at the global scale, providing data up to a daily frequency for eruptive emissions, and a yearly frequency along with the annual uncertainty for passive emissions.

These new global volcanic sulfur inventories open the possibility of new, more detailed and accurate studies of the impact of volcanic emissions at the global scale; a stark improvement compared with studies of the last decades widely focused on major volcanic eruptions [Robock (2000)]. At the global scale, numerous studies aim at the assessment of the dispersion of sulfate aerosols and the subsequent radiative forcing [Graf et al. (1997, 1998), Gasso (2008), Ge et al. (2016)]. Regarding their impact on tropospheric composition, including air quality, several case studies at the regional scale have been analysed [e.g., Colette et al. (2010), Schmidt et al. (2015), Boichu et al. (2016, 2019), Sellitto et al. (2017)] but very few studies at the global scale have been conducted [Chin and Jacob (1996), Sheng et al. (2015), Feinberg et al. (2019)].

In this context, the objective of this work focuses on the study at the global scale of the impact of volcanic sulfur emission on the tropospheric composition, the surface concentration and the deposition of sulfur species. We aim to assess and to analyse the contribution of volcanoes to the global sulfur budget using a Chemistry-Transport Model (CTM). Here, we use the MOCAGE CTM, developed at the Centre National de Recherches Météorologiques (CNRM) [Josse et al. (2004), Guth (2015)]. Firstly, we will evaluate the changes induced by the update of the volcanic sulfur emission inventory into MOCAGE; namely from the inventory of Andres and Kasgnoc (1998) to the one of Carn et al. (2016, 2017). Secondly, the focus will be on the analysis of the volcanic SO₂ and sulfate aerosol tropospheric distribution and contribution, at the global scale, as well as the sulfur species concentration and deposition at the surface.

In Section 2, we present the configuration of simulations with the MOCAGE CTM. The new volcanic SO₂ emission inventory and its upgrades compared to the Andres and Kasgnoc (1998) one are described in Sect. 3. In Sect. 4 the setup of the simulations and the observations used to evaluate them are presented. The evaluation of the updated inventory is presented in Sect. 5. In Sect. 6, the comparison of the tropospheric and surface species concentrations between the simulations is analysed. Next, the new sulfur species distribution and budget in the atmosphere are analysed in Sect. 7. A sensitivity analysis on the passive emission sources based on the annual uncertainties provided in the Carn's inventory is carried out in Sect. 8. Finally in Sect. 9, a conclusion is given.

2 Description of MOCAGE model

2.1 General features

MOCAGE (Modèle de Chimie Atmosphérique à Grande Échelle) is an off-line global and regional three-dimensional chemistry-transport model developed at CNRM [Josse et al. (2004), Guth (2015)]. It is used for various scientific topics: impact of climate

change on atmospheric composition [e.g. Teyssède et al. (2007), Lacressonnière et al. (2014, 2016, 2017), Lamarque et al. (2013)], chemical exchanges between the stratosphere and the troposphere using data assimilation [e.g. El Amraoui et al. (2010), Barré et al. (2012)], operational production of air quality forecasts for France (Prev' Air program [Rouil et al. (2009)])
95 and for Europe (as one of the nine models contributing to the regional ensemble forecasting system of the Copernicus Atmosphere Monitoring Service (CAMS) European project [Marécal et al. (2015); <https://atmosphere.copernicus.eu/>]).

A special feature of the model makes possible to include a natural or anthropogenic accidental source, such as volcanic eruptions or nuclear explosions, during a simulation. This feature is used as part of the Toulouse VAAC (Volcanic Ash Advisory Center) of Météo-France, which is responsible for monitoring volcanic eruptions over a large area (including part of Europe
100 and Africa). In order to input an accidental emission, it is required to input the time and place (latitude/longitude), the bottom and top plume heights, the total quantity emitted as well as the duration of the emission.

2.2 Model geometry and inputs

The CTM MOCAGE can be used with global or regional resolutions based on its grid nesting capability. Each outer domain forces the inner domain at its edges (boundary conditions). The global domain has a typical resolution of 1° longitude x
105 1° latitude (around 110 km x 110 km at the equator and 110 km x 80 km at mid-latitudes), while the regional domain resolutions are typically 0.2° longitude x 0.2° latitude (around 22 km x 16 km at mid-latitudes) and 0.1° longitude x 0.1° latitude resolution (around 11 km x 8 km at mid-latitudes).

The vertical grid has 47 levels from the surface to 5 hPa (about 35 km), with 7 levels in the planetary boundary layer, 20 in the free troposphere and 20 in the stratosphere. The vertical coordinates are expressed in σ -pressure; meaning that the model
110 levels follow closely the topography in the low atmosphere and the pressure levels in the upper atmosphere.

Being an off-line model, MOCAGE gets its meteorological fields (wind speed and direction, temperature, humidity, pressure, rain, snow and clouds) from an independent numerical weather prediction model. In practice, they can come from two meteorological models at the global scale: the IFS model (Integrated Forecast System) operated at the ECMWF (European Center for Medium-Range Weather Forecast System, <http://www.ecmwf.int>) or from ARPEGE model (Action de Recherche
115 Petite Echelle Grande Echelle) operated at Météo-France [Courtier et al. (1991)].

2.3 Emissions

At the global scale, anthropogenic emissions from the MACCity inventory are used [Lamarque et al. (2010)], while biogenic emissions for gaseous species are from the MEGAN-MACC inventory, also representative of the year 2010 [Sindelarova et al. (2014)]. Note that the difference between 2010 and 2013 emissions is negligible for the purpose of this study, SO_2 emissions
120 being only about 1% higher in 2010 than in 2013. Nitrogen oxides from lightning are based on Price et al. (1997) and configured dynamically according to the meteorological forcing. Organic and black carbon are taken into account following MACCity [Lamarque et al. (2010)]. DMS oceanic emissions are a monthly climatology [1° horizontal data Kettle et al. (1999)]. Finally, the daily biomass burning emissions available for each day in 2013 come from the GFAS daily products [Kaiser et al. (2012)]. Volcanic emissions are discussed in detail in Sect. 3.

125 In MOCAGE, with the exception of the species emitted from biomass burning [Cussac et al. (2020)], lightning NO_x [Price
et al. (1997)] and aircraft [Lamarque et al. (2010)], all of the chemical species sources are injected in the first five levels
of the model (up to approximately 500 m). This configuration is necessary for the numerical stability in the lowest model
levels. The injection profile implemented follows an exponential decrease from the surface level of the model (including model
orography): $\delta_L = 0.5\delta_{L-1}$, with δ_L the injection fraction of the mass emitted at the level L of the model. It means that the
130 majority of pollutants are emitted at the surface level and then quickly decrease with altitude. Hereafter, we will refer to "the
model surface" when this configuration is used.

2.4 Chemistry and aerosols

2.4.1 Gaseous species

The MOCAGE chemical scheme is named RACMOBUS. It merges two chemical schemes representing the tropospheric and
135 stratospheric chemistry. The first one, the Regional Atmospheric Chemistry Mechanism (RACM) [Stockwell et al. (1997)],
completed with the sulfur cycle [details in Guth et al. (2016)], represents tropospheric species and reactions. The second one,
REactive Processes Ruling the Ozone BUDget in the Stratosphere (REPROBUS), provides the additional chemistry reactions
and species relevant for the stratosphere, in particular long-lived ozone depleting substances [Lefèvre et al. (1994)].

A total of 112 gaseous compounds, 379 thermal gaseous reactions and 57 photolysis rates are represented in MOCAGE. The
140 calculation of the reaction rates is performed during the simulation every 15 min. The photolysis reaction rates are interpolated
on the same 15-minute time step from a look-up table from the TUV model [Madronich (1987)]. [The TUV model calculates
photo-dissociation rates for both the troposphere and stratosphere.](#) A modulation at each grid point and for all time iterations
is applied as a function of the ozone column, solar zenith angle, cloud cover and surface albedo.

2.4.2 Aerosols

145 Both primary and secondary aerosols are represented in the model [Martet et al. (2009), Sič et al. (2015), Guth et al. (2016),
Descheemaeker et al. (2019)]. All types of aerosols use the same set of six sectional size bins, ranging from 2 nm to 50 μm
(with size bins limits of 2, 10, and 100 nm, and 1, 2.5, 10 and 50 μm).

Primary aerosols are composed of four species: black carbon, primary organic carbon, sea salt and desert dust. The first two
species (black and organic carbon) depend on emission inventories while sea salts and desert dusts are dynamically emitted
150 using the meteorological forcing at the resolution of each domain [Sič et al. (2015)].

Secondary inorganic aerosols (SIA) are implemented in MOCAGE [Guth et al. (2016)]: sulfate, nitrate and ammonium
aerosols. The thermodynamic equilibrium model ISORROPIA (precisely the latest version ISORROPIA II) [Nenes et al.
(1998), Fountoukis and Nenes (2007)] is used to calculate SIA concentrations in MOCAGE depending on the partition of
compound concentrations, the gaseous and aerosol phases, and the ambient conditions (temperature, pressure).

155 Secondary organic aerosols are treated in MOCAGE similarly to primary aerosols with its emissions scaled on the primary
anthropogenic organic carbon emissions. The scaling factor is derived from aerosol composition measurements [Castro et

al. (1999)]. The implementation in MOCAGE was done by Descheemaeker et al. (2019) in the frame of a study on data assimilation for air quality applications.

2.5 Transport

160 The transport in the model is solved in two steps. A first one explicitly determines the large-scale transport (advection) with the wind input data provided by the forcing weather model. For this purpose, a semi-Lagrangian scheme is used [Williamson and Rasch (1989)]. The second step represents the sub-grid phenomena that cannot be solved explicitly, such as convection and turbulent scattering. The convective transport is configured upon Bechtold et al. (2001) set-up. The scheme of Louis (1979) is used to diffuse the species by turbulent mixing.

165 3 Volcanic sulfur emissions in the model

Volcanic emissions are composed of several gases, with the chemical composition changing from one volcano to another, depending on the geodynamical context. Sulfur species emitted by volcanoes are mainly sulfur dioxide (SO₂), and hydrosulphuric acid (H₂S) in much lower quantity. Being by far the dominant sulfur species, only SO₂ is referenced in global inventories of volcanic emissions.

170 3.1 Previous volcanic sulfur inventory

The previous inventory implemented in MOCAGE is from Andres and Kasgnoc (1998), which is a study contributing to the work of GEIA. Measurements ranged over a period of about 25 years, from the early 1970s to 1997, and covered volcanic SO₂ emissions at the global scale.

A synergy between the COSPEC surface instrument and the TOMS satellite instrument was used. The COSPEC is a correlation spectrometer initially used in pollution measurements [Moffat and Millan (1971), Williams-Jones et al. (2008)]. However, vulcanologists have adapted it to measure the quantities of sulfur dioxide in a moving air mass (here the volcanic plume). It works by comparing the amount of solar ultraviolet (UV) radiation absorbed in the plume with a standard (one sample of the background sky and two laboratory-calibrated SO₂ concentration cells). It is most commonly used under quiet to moderate eruptive conditions. On the contrary, the space instrument TOMS [Krueger et al. (1995), Seftor et al. (1997), Torres et al. (1998a)], operational between 1978 and 2005, was able to detect larger eruptions. The synergy of these two instruments is therefore complementary in the development of the inventory. Although the first instrument is better adapted to the measurement of weak flares and the second to the strongest ones, a campaign dedicated to Popocatepetl in Mexico showed the good correlation between the two instruments [Schaefer et al. (2011)].

185 Measurements were only carried out on sub-aerial volcanoes, *i.e.*, emitting gases directly into the atmosphere. A total of 69 volcanoes are listed in the inventory, divided into two categories: 49 continuously erupting volcanoes and 25 sporadically erupting volcanoes. Five volcanoes belong to both categories because they had a main activity of continuous emission and also sporadic eruptive events: Aso, Augustine, Kilauea East Rift Zona, Mayon and San Cristobal.

Since the beginning of volcanic emission measurements in the early 1970s, the global activity of continuous eruptions has shown relative stability. The fluxes provided in the inventory correspond to a temporal average of all measurements for each volcano. Only three volcanoes are not concerned by this hypothesis: Etna in Sicily, Kilauea and the Kilauea Rift Zone in Hawaii, which are known as being among the largest emitters of SO₂. For those volcanoes, fluxes provided by specific studies [personally communicated to Andres and Kasgnoc (1998)] supersede the averages.

Since sporadic eruption data in Andres and Kasgnoc (1998) are not recent, it is not possible to take them into account for the recent year chosen for the MOCAGE simulation. Therefore, only continuous eruptions are used in MOCAGE and a global time-averaged SO₂ flux of 13 Tg yr⁻¹ is reported.

Since no configuration was developed in MOCAGE to inject volcanic emissions aloft until this study, they were implemented similarly as the other pollution sources. Volcanic SO₂ were thus emitted at the model surface (see Sect. 2.3). However, the surface elevation of the model (orography) is mainly below the actual elevation of the volcanoes.

3.2 New volcanic sulfur inventory

With the improvements in satellite technology, an increasing number of satellites are now able to better detect the sources of volcanic SO₂: plume heights, quantities emitted and location. The most recent instruments with respect to TOMS, such as the Ozone Monitoring Instrument (OMI) and the TROPOspheric Monitoring Instrument (TROPOMI) [Theys et al. (2019)], have a higher sensitivity to detect small eruptions, but also passive degassing. Global coverage gives another considerable advantage over other measurement techniques. As a reminder, COSPEC carries out measurements from the ground and cannot be deployed on hard-to-access volcanoes.

The work of Carn et al. (2016, 2017) updates and adds complementary information to the study of Andres and Kasgnoc (1998) with a new inventory. The inventory is divided into two parts corresponding to the two types of emissions detectable by satellites.

Firstly, the eruptive emissions dataset [Carn et al. (2016) data available in Carn (2019)] is a synthesis of 40 years of daily SO₂ measurements (between 31/10/1978 and 31/12/2018) derived from 7 satellite instruments: TOMS, OMI and OMPS (Ozone Mapping and Profiler Suite) in the ultraviolet (UV), TIROS Operational Vertical Sounder (TOVS), Atmospheric InfraRed Sounder (AIRS) and Infrared Atmospheric Sounding Interferometer (IASI) in the infrared (IR) and the Microwave Limb Sounder (MLS) in the microwave range. Data from 119 volcanoes and a total of 1502 events over the period are provided. For each of these eruptions, the information given includes the location of the volcano (latitude and longitude), the date, the VEI (Volcanic Explosivity Index), the estimated SO₂ mass released (in kt), but also the height of the volcano and the height of the plume (measured if possible, estimated if not). Within our study, the additional information from Carn et al. (2016) on the injection height is used (see details here after), taking into account the height of the volcano as the base of the emissions and the height of the plume as the top of the injection.

Secondly, the passive degassing dataset is the first documented volcanic sulfur dioxide emission inventory made with global satellite measurements [Carn et al. (2017)]. It was retrieved from the observations of the OMI instrument in the UV spectrum during a long-term mission between 2005 and 2015. The high sensitivity of the instrument was a technological breakthrough

that made it possible to distinguish low SO₂ sources; 30 kt/y for persistent anthropogenic sources and lower (6 kt/y) for volcanoes which are located at higher altitudes or at lower latitudes that benefit from more satellite observations and optimal conditions (low solar zenith angle). The volcanic SO₂ sources have been identified on the basis of 3-year averages (2005-2007, 225 2008-2010, 2011-2014), which implies that for a source to be characterized as persistently degassing, the emission must be relatively constant on this time scale. Annual mean emissions were calculated for each 90 volcanic source identified over the 11 years of the study. We assume in the model that emission fluxes are constant throughout the year.

Several parameters can affect the retrieval of volcanic emissions; the measurement process, the calculation algorithm or from the characterization of the type of emission. Thus, annual uncertainties are given with the mean annual emissions, for 230 each volcanoes and each year. The total uncertainty of annual sulfur dioxide fluxes are estimated at 55 % and over 67 % for sources emitting more than 100 kt/y and less than 50 kt/y, respectively. This latter information is exploited in the sensitivity analysis (see Sect. 8). Note also that depending on the instrument used, the retrieval of the plume altitude can differ. Therefore, there are uncertainties on the altitude information provided by the inventory.

Information on the altitude of volcanoes and on the plume height in the Carn et al. (2016) inventory is used to implement a 235 configuration to inject volcanic emissions aloft, rather than at the model surface. This is an important improvement, knowing that in some areas, depending on the model resolution chosen, the model orography may differ from the actual topography and have an impact on the transport of volcanic emissions. The new implementation sets the passively degassing emissions at the model level of the volcano altitude. For eruptions, the mass of SO₂ emitted is distributed from the model level at the volcano vent to the model level of the plume top height and follows an "umbrella" profile similar to that used in other chemistry 240 models (Freitas et al. (2011) and Stuefer et al. (2013)). During a volcanic eruption, the emitted materials (ashes and gases) are rapidly transported vertically by the convection in the plume and most of the materials is concentrated at high altitude, giving an "umbrella" profile. In practice, the plume follows an almost linear profile with increasing altitude from the volcano vent and then opens into a parabola containing 75 % of the gases in mass into the top third of the plume.

In summary (see Table 1), the updated volcanic sulfur emission inventory includes now about 160 volcanoes (110 in the 245 eruptive category and 90 in the passive degassing category with 40 volcanoes in common). The availability of plume heights in this inventory allows a better representation of the injection of the volcanic emission in the model.

4 Simulation set-ups and observations

4.1 Description of the simulations

Meteorological fields are driven by the ARPEGE 3-hourly forecasts. Anthropogenic and biomass burning sources emit SO₂, 250 whereas biogenic emissions from the ocean are assumed to occur as DMS. Oceanic DMS emissions are 19.9 Tg S yr⁻¹, while anthropogenic emissions are 48.6 Tg S yr⁻¹. For 2013, biomass burning emissions from GFAS products were relatively low, only 1 Tg S yr⁻¹.

Table 1. Summary of the main characteristics of the previous [Andres and Kasgnoc (1998)] and the updated [Carn et al. (2016, 2017)] SO₂ volcanic emission inventories.

	Previous Volcanic Inventory		New Volcanic Inventory	
	Andres and Kasgnoc (1998)	Carn et al. (2016)	Carn et al. (2017)	
Emission type	Continuous emissions	Eruption	Passive degassing	
Period	1970-1997	1978-2018	2005-2018	
Instruments	COSPEC & TOMS	7 satellite instruments	OMI	
Frequency	Time averaged over the period	Daily total quantity per volcano	Annual mean quantity per volcano	
Information on the vertical	no information	volcano altitude	volcano altitude & plume height	
Number of volcanoes	43	119	91	

Table 2. Main features of the simulations.

	Volcanic inventory	Altitude of injection
REF	Andres and Kasgnoc (1998)	at model surface
CARNALTI	Carn et al. (2016) - eruption	from volcano vent to plume top
	Carn et al. (2017) - degassing	at volcano vent
CARN	Carn et al. (2016, 2017)	at model surface
NOVOLC	N/A	N/A

Concerning volcanic sulfur emission inventories, either Andres and Kasgnoc (1998) or Carn et al. (2016, 2017) are used. The full eruption emission database is available following Carn (2019) (https://disc.gsfc.nasa.gov/datasets/MSVOLSO2L4_3/ summary).

Four different simulations (Table 2) are carried out in order to evaluate the impact induced by the update of the volcanic SO₂ inventory in MOCAGE and to analyse its contribution to the sulfur species budget in the atmosphere at the global scale. The four simulations are run at a resolution of 1° x 1°.

The first simulation, named REF, takes into account the previous volcanic inventory [from Andres and Kasgnoc (1998)] with the injection at the model surface. The second simulation, named CARNALTI, uses the updated volcanic inventory [from Carn et al. (2016, 2017)] and the new configuration to inject volcanic emissions from the volcano altitude as described in Section 3.2. By comparing REF and CARNALTI runs, we can analyse the changes brought by the updated volcanic emission inventory with respect to the previous one. These two simulations are evaluated in Section 5 and the associated global distribution of sulfur species is compared in Section 6.

In order to distinguish between the impact of the height of emission and of the quantity of SO₂ emitted, another simulation, named CARN is run and used for the analysis of the differences between REF and CARNALTI global distribution of sulfur

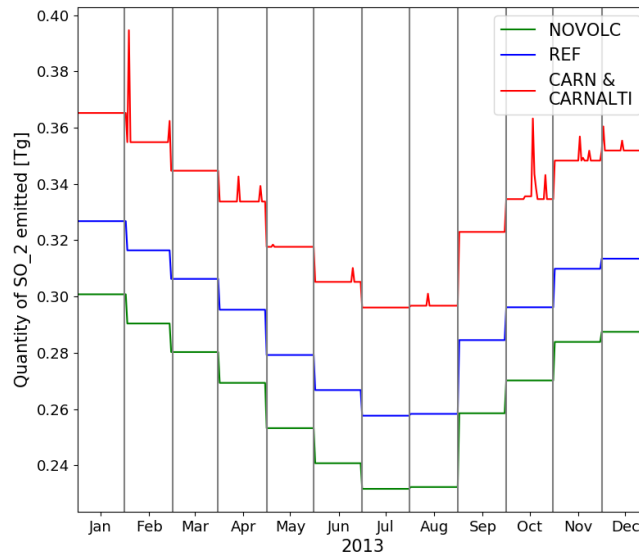


Figure 1. Temporal evolution of 2013 SO_2 emissions in Tg; non-volcanic emissions inventory for NOVOLC, plus Andres and Kasgnoc (1998) volcanic emissions inventory in REF or Carn et al. (2016, 2017) volcanic emissions inventory in CARN and CARNALTI.

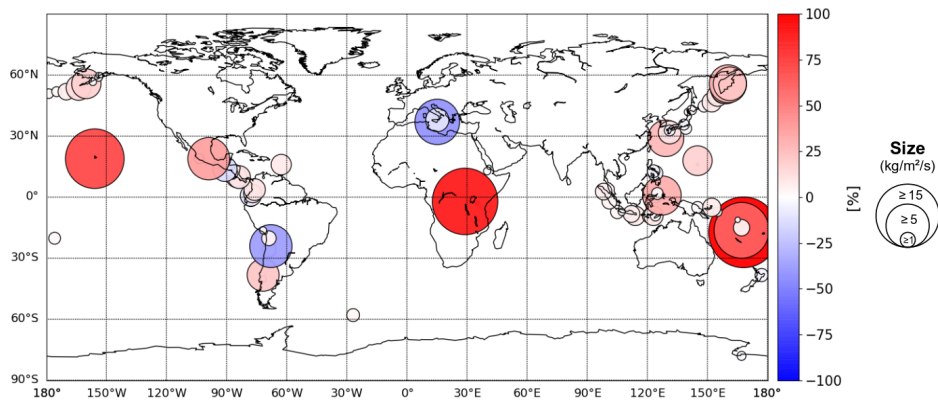


Figure 2. 2013 annual average ratio between volcanic SO_2 emissions in Carn et al. (2016, 2017) and Andres and Kasgnoc (1998) inventories. The size of the circles represents the absolute difference in $kg/m^2/s$ while the color represents the relative difference in %.

species. Volcanic emissions are from Carn et al. (2016, 2017), like in CARNALTI but they are injected at the model surface, like in REF.

270 CARNALTI is run to provide a better representation of the global tropospheric sulfur. This is why it is selected for the analysis of the tropospheric sulfur budget in Section 7. In order to quantify the contribution of the volcanoes in the sulfur budget, we compare CARNALTI to the NOVOLC simulation that does not take into account volcanic emissions (only anthropogenic, biomass burning and dust).

The four simulations are run for the year 2013 with a 3 month spin-up period (from October to December 2012). In addition to being one of the years when a large amount of observational data is available globally, 2013 is chosen as the year with the lowest eruptive emission flux (Carn et al. (2016)). Figure 1 shows the volcanic emissions of the different simulations for the year 2013. We notice the monthly variation due to non-volcanic emissions (NOVOLC run in green), with less emissions during the northern hemisphere summer and the highest values in the northern hemisphere winter. Volcanic emissions from Andres and Kasgnoc (1998) are steady throughout the year, as we can see in REF run (in blue). They are lower than the volcanic emissions of CARNALTI and CARN runs (in red), with strong constant passive degassing throughout the year and a few sporadically eruptive events. Indeed, Andres and Kasgnoc (1998) SO₂ emissions are 13 Tg (or 6.5 Tg S), while the total 2013 annual emissions in Carn et al. (2016, 2017) are 23.7 Tg of SO₂ (or 11.8 Tg S), with 23.5 Tg of passive degassing SO₂ and 0.2 Tg of eruptive emission (< 1 % of the total amount of volcanic SO₂ emission, almost negligible).

Figure 2 represents spatially the difference between the previous and the new inventories. The red dots mostly show new volcanoes in Carn et al. (2016, 2017), not accounted for by Andres and Kasgnoc (1998). However, we also notice blue dots, meaning that in the new inventory, the estimated emission fluxes are reduced. Given the low number of eruptive emissions in 2013, the annual average of volcanic emissions in Fig. 2 essentially represents passive emissions.

4.2 Observations used for the evaluation of the simulations

We use for the model evaluation satellite-based instruments since they provide a global sampling. The target chemical species that we evaluate are SO₂ and aerosols, since SO₂ is the precursor of sulfate aerosols. Concerning SO₂, observations in the infrared are not suitable since passive degassing are mostly under 5 km, at altitude where such instruments have reduced sensitivity [Carboni et al. (2012), Taylor et al. (2018)]. Therefore, observations in UV-Visible are chosen. GOME-2 Metop A instrument being at the end of its lifetime, data retrievals are not good enough and presents strong artefacts, as for GOME-2 Metop B. Therefore we choose the Ozone Monitoring Instrument (OMI) instrument, being the most widely used (*e.g.* He et al. (2012), Fioletov et al. (2013), Wang et al. (2017), Wang and Wang (2020)). Moreover, the SO₂ the tropospheric column estimated from the OMI is the finest resolution and most accurate instrument in 2013 to retrieve SO₂ total columns over passively emitted volcanoes whose altitudes are generally around 2-3 km. For aerosols, there is no satellite-derived product providing information on sulfate only. Nevertheless, satellite observations of aerosols as a whole are available. Here, we choose MODIS (Moderate-Resolution Imaging Spectroradiometer) aerosol optical depth (AODs) which provides data at the global scale. MODIS AODs are known as being a robust product used in the literature for global evaluation and aerosols assimilation in models (*e.g.*, Li et al. (2011), Dai et al. (2014), Sič et al. (2015), Guth et al. (2016, 2018)). The model comparison with MODIS AODs provides an indirect evaluation for sulfate aerosols since AODs include sulfate aerosols.

4.2.1 OMI SO₂ total column

The Aura Ozone Monitoring Instrument (OMI) level 2 sulphur dioxide (SO₂) total column product [Li et al. (2020)] was used to validate the model simulations. This product is available since 2004. The resolution of the data is 13 km x 24 km at nadir. The

305 retrieval algorithm is a principal component analysis (PCA)-based algorithm [Li et al. (2013)]. Various physical and technical causes can reduce the quality of data. Thus a pre-processing and data filtering was applied as recommended to select only the best possible observations. Pixels with large solar zenith angles (SZAs > 65°), affected by the South Atlantic Anomaly region [Richter et al. (2006)], on the edge of the swaths or the OMI row anomaly (signal suppression at certain OMI rows; see Schenkeveld et al. (2017)), pixels with a cloud fraction greater than 30% or flagged with low-confidence data are removed.

310 There are various products available in the OMI dataset since the OMI instrument has a variable sensitivity depending on altitude and the retrieval of SO₂ requires the use of an *a priori* profile. The first product selected, named "Column_Amount_SO₂", is an estimate of SO₂ vertical column density (VCD) and constrained by the GEOS-5 global model *a priori* profiles. Then, three specific products with adapted *a priori* profiles are also available and selected. One named "Column_Amount_SO₂_PBL" is an estimate of SO₂ VCD with an *a priori* profile assuming that the essential of SO₂ is in the boundary layer (within the low-
315 est 1 km of the atmosphere). Another product named "Column_Amount_SO₂_TRL", is almost the same as the previous one, but assuming a lower tropospheric SO₂ profile (with a center of mass altitude at 3 km). The last product selected, named "Column_Amount_SO₂_TRM", corresponds to an assumed middle tropospheric SO₂ profile (with a center of mass altitude at 8 km).

4.2.2 MODIS Aerosol Optical Depth

320 We use daily level 3 MODIS data (MOD08 (Terra), MYD08 (Aqua), collection 6.1) for the year 2013. Before use, we performed additional quality control and screening (Sič et al. (2015), Guth et al. (2016)). These treatments aims at minimizing cloud contamination and avoid low confidence measurements [Zhang et al. (2005), Koren et al. (2007), Remer et al. (2008)]. Moreover, all AOD values below 0.05 are automatically filtered out because Ruiz-Arias et al. (2013) highlighted the rapid growth in the relative underestimation of AODs after this threshold which leads to a mean relative error above 50 %.

325 In MOCAGE, AODs are calculated using Mie theory with the Global Aerosol Data Set's refractive indices [Köpke et al. (1997)] and extinction efficiencies derived with the Mie scattering code for homogeneous spherical particles from Wiscombe (1980).

4.3 Statistical metrics used for evaluation

In order to evaluate the model against observation data, we use the fractional bias, the fractional gross error, the root-mean-square error and the correlation coefficient, following Seigneur et al. (2000).
330

The fractional bias or modified normalized mean bias (MNMB) quantifies the mean between the modelled (f) and the observed (o) elements, for N observations. It ranges between -2 and 2 and varies symmetrically with respect to under and overestimation of the model. The definition is given by:

$$MNMB = \frac{2}{N} \sum_{i=1}^N \frac{f_i - o_i}{f_i + o_i} \quad (1)$$

335 The fractional gross error (FGE) quantifies the model error. It is a positive variable ranging between 0 and 2. The definition is given by:

$$FGE = \frac{2}{N} \sum_{i=1}^N j \frac{f_i - o_i}{f_i + o_i} j \quad (2)$$

The root-mean-square error (RMSE) is the square root of the average of the squared difference between each model and observation value. In other words, it represents a measure of the accuracy in absolute values while FGE is relative. RMSE is a positive variable, and a value of 0 (almost never achieved in practice) would indicate a perfect fit to the data. The formula is given by:

$$RMSE = \sqrt{\frac{1}{N} \sum_{i=1}^N (f_i - o_i)^2} \quad (3)$$

The correlation coefficient (R) indicates whether the variations of the model and the observations are well matched and ranges between -1 and 1. The closer the score is to 0, the weaker the correlation is. The definition is given by:

$$R = \frac{\frac{1}{N} \sum_{i=1}^N (f_i - \bar{f})(o_i - \bar{o})}{\sigma_f \sigma_o} \quad (4)$$

where \bar{f} and \bar{o} are, respectively, the model and observations mean values, and σ_f and σ_o are the standard deviations from the modelled and observed time series.

5 Evaluation of the simulations

350 5.1 Evaluation strategy

For the evaluation of the simulations, OMI and MODIS dataset are mapped at the model resolution ($1^\circ \times 1^\circ$). The model grid points in the simulations corresponding to the filtered observation pixels (as explained in Sect. 4.2.1 and Sect. 4.2.2) are also removed. A different validation strategy is applied depending on the instrument.

Concerning OMI SO₂ total columns, similarly to other SO₂ satellite derived products, their relative uncertainties are large where the signal is low, in particular for background conditions. This is why in the literature, the SO₂ satellite comparisons and the model evaluations focus on specific areas close to SO₂ sources [*e.g.* He et al. (2012), Fioletov et al. (2013), Wang and Wang (2020)]. Similarly to these studies, our strategy is to perform the model evaluation only in the vicinity of the volcanic sources. For each volcano, based on those referenced in Carn et al. (2016, 2017), we select 9 model grid points (representing a square of $3^\circ \times 3^\circ$) with the middle point being where the volcano is located (see Figure 3). Altogether it corresponds to 633 points. The mask is applied on each daily OMI SO₂ total column measurements and then we perform an annual average for each of the 633 data points. Similarly to the above mentioned studies, the results are shown as scatter plots and the statistical metrics used are the correlation coefficient and the RMSE.

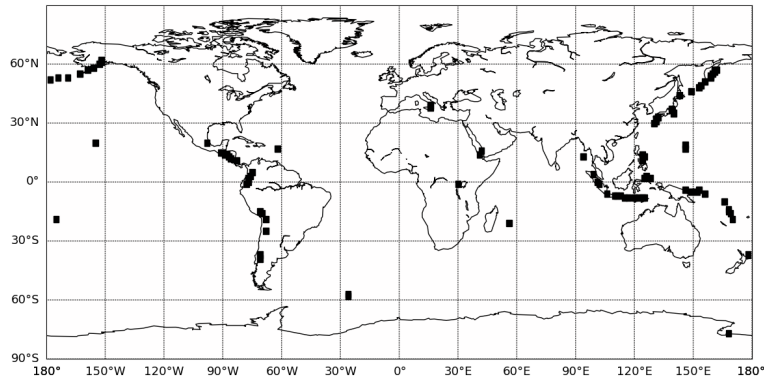


Figure 3. Location of the selected areas where OMI SO_2 total column are selected for the validation. They correspond to 9 MOCAGE grid points around each volcano from Carn et al. (2016, 2017).

Two methods are used in the evaluation strategy. Firstly, we choose to evaluate the model SO_2 total column against OMI "Column_Amount_ SO_2 " product. However, in order to test if the evaluation is sensitive to this choice, we use another approach which consists in an interpolation of OMI SO_2 observations at the altitude where the volcanic emissions are injected in MOCAGE. To do so, we use OMI products "Column_Amount_ SO_2 _PBL", "Column_Amount_ SO_2 _TRL" and "Column_Amount_ SO_2 _TRM", renamed hereafter "PBL", "TRL" and "TRM" respectively. Depending on the altitude of the emissions in MOCAGE, either "PBL" and "TRL", or "TRL" and "TRM", are used for the interpolation.

Concerning the AODs, a spatial validation on the whole global domain is possible against MODIS products. The evaluation at the global scale enables us to quantify the overall aerosol changes in the simulations from the use of the updated inventory with respect to the previous one. Since noticeable changes are also expected at the local scale, in the vicinity of the volcanoes, three zones are selected to complete the global scale evaluation against MODIS. These zones are chosen among the largest passive SO_2 emitters in Carn et al. (2017) and are representative of different types of changes between Andres and Kasgnoc (1998) and Carn et al. (2016, 2017) volcanic emissions inventories.

Zone 1 is centered over Central Africa and under the influence of the Nyiragongo and Nyamuragira (alt. 2950 m). In Andres and Kasgnoc (1998), this volcano is not listed. In contrast, in Carn et al. (2017), the passive degassing emission represents 2.29 Tg in 2013. No eruption is listed in Carn et al. (2016) for 2013.

Zone 2 is located in the North Pacific Ocean, around Hawaii. The volcano, based on the island, is the Kilauea (alt. 1222 m). In the REF simulation, the volcano emissions in the inventory are 0.45 Tg yr^{-1} (7 th rank of the most SO_2 -emitting volcanoes in Andres and Kasgnoc (1998)). But in Carn et al. (2017), the Kilauea emissions are updated and it is the second biggest emitter with 2.17 Tg. In 2013, no eruption are recorded in Carn et al. (2016) for this area.

Zone 3 is located in the Mediterranean region, under the influence of the Etna (alt. 2711 m in the inventory) and Stromboli (alt. 870 m in the inventory). In Andres and Kasgnoc (1998), 1.48 Tg yr^{-1} are emitted by the Etna (the biggest volcanic SO_2 emitter referenced), 0.27 Tg yr^{-1} are emitted by the Stromboli and also 0.02 Tg yr^{-1} by the Vulcano. In Carn et al. (2016, 2017),

Table 3. 2013 annual statistics of REF and CARNALTI simulations against MODIS observations on specific zones.

	Globe			Zone 1			Zone 2			Zone 3		
	MNMB	FGE	R	MNMB	FGE	R	MNMB	FGE	R	MNMB	FGE	R
REF	0.10	0.44	0.33	-0.53	0.61	0.70	0.31	0.34	0.75	0.74	0.75	0.61
CARNALTI	0.15	0.43	0.35	-0.28	0.41	0.72	0.47	0.48	0.78	0.73	0.74	0.64

385 only 0.65 Tg of SO₂ are emitted in 2013 in the Zone 3; corresponding to less than 0.04 Tg for Stromboli and 0.61 Tg for the Etna. The Vulcano is not in the Carn et al. (2016, 2017) inventories. In 2013, small eruptions have occurred at Etna, totalling a little less than 0.06 Tg. Therefore, in the updated Carn et al. (2016, 2017), volcanic emissions in Zone 3 are weaker than in Andres and Kasgnoc (1998).

390 For the evaluation of the simulations against MODIS, the statistical metrics used are the MNMB, FGE and correlation coefficient. MNMB and FGE being dimensionless, they are meaningful in all geographical regions regardless of the magnitude of the aerosol column.

5.2 Validation against OMI SO₂ total column

Figure 4 (top row) presents the scatter plots of MOCAGE SO₂ columns in DU from the REF and CARNALTI simulations against OMI observations based on GOES-5 *a priori* profiles. Each of the points represents an average over the 2013 year. Fig. 395 4 shows that the previous version of the model (REF) was not good. The coefficient correlation is low (0.12). The bias is high with a mean SO₂ measured by OMI of 0.28 DU, and of 0.08 in REF simulation. With the new volcanic inventory in CARNALTI simulation, the mean SO₂ concentration is still below OMI retrievals (0.17 DU) but much closer. We can also clearly see an improvement of the model performances with a reduced RMSE and a correlation increased up to 0.68.

To evaluate the impact of the choice of OMI product, we also show in Fig 4 (bottom row) the scatter plot when applying 400 the interpolation at the MOCAGE altitude where volcanic emissions are injected. This method provides higher OMI estimates and therefore increases the bias with MOCAGE simulations but also improves the correlation. The conclusion is that the CARNALTI simulation provides by far better statistical results (bias, RMSE and correlation) than REF. The negative bias of MOCAGE CARNALTI with respect to OMI could be due to errors in the plume transport in the model linked to uncertainties in the meteorological inputs, to the limited number of model vertical levels, to the model chemistry/aerosol scheme but also to 405 the uncertainties in the SO₂ emission estimates from OMI in Carn et al. (2016, 2017) and in the OMI retrieval products used for the model evaluation.

5.2.1 Validation against MODIS AOD at 550 nm

As a second evaluation step, we compare the simulations' AOD with the AOD from MODIS. Figure 5 presents for REF and CARNALTI experiments, the 2013 annual MNMB with respect to MODIS AOD observations. We can see that the equatorial

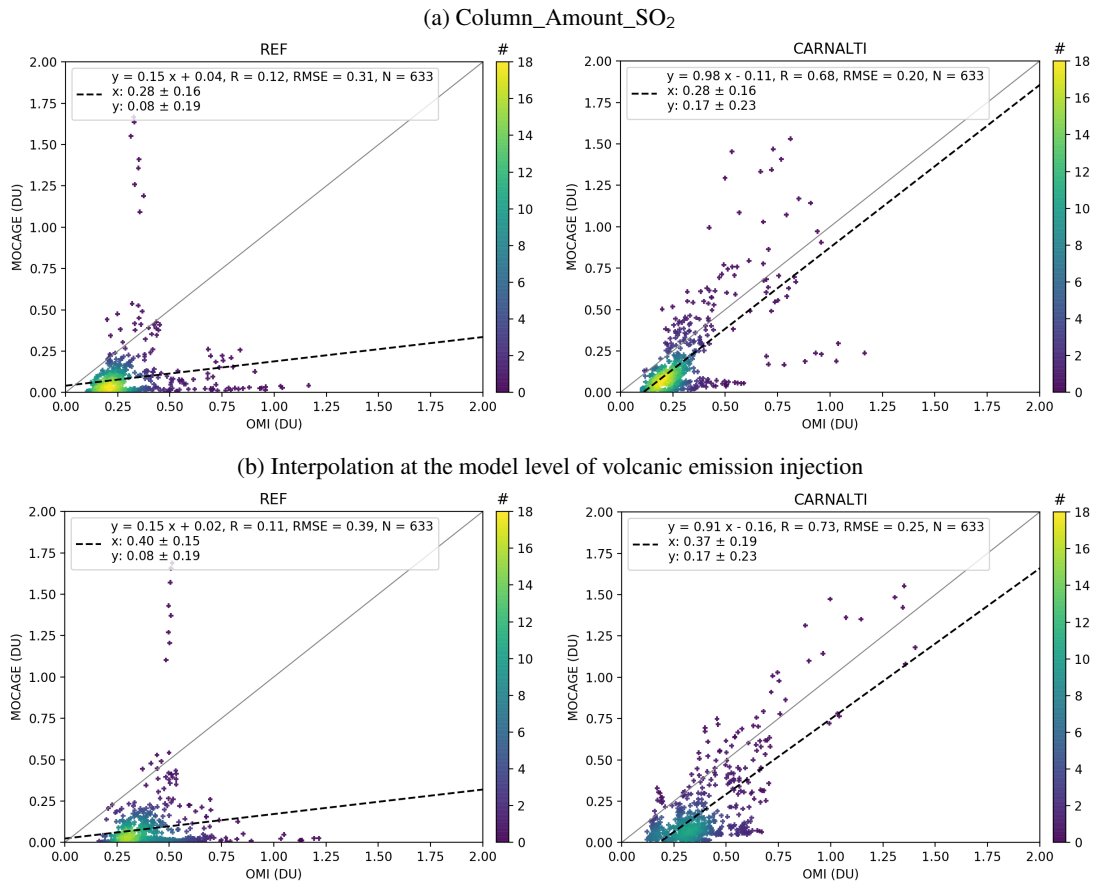


Figure 4. Scatter plots of annual mean OMI SO₂ versus MOCAGE simulations (left: REF, right: CARNALTI) (a) considering total columns and (b) interpolating at the model level where volcanic emissions are injected. Also shown on the scatter plot are 1:1 line (solid grey), linear regression line (black dash), linear regression formula, correlation coefficient (R), root mean squared error (RMSE), number of collocated pairs (N), OMI mean and standard deviation in DU (x), MOCAGE mean and standard deviation in DU (y), and density of collocated pairs (colorbar).

410 belt has a negative MNMB, between -0.2 and -1.2 in REF simulation, but in CARNALTI simulation, it is closer to 0; *e.g.*, in the vicinity of volcanoes in Indonesia or in central Africa. This shows an improvement of the MOCAGE AOD modeling at the global scale by updating the volcanic emissions inventory. Despite the improvement in MNMB in the areas near volcanoes, the overall score is not improved (see Table 3). Indeed, the MNMB of the Northern Hemisphere is mainly positive and almost unchanged with the new inventory [Carn et al. (2016, 2017)] where only a few volcanoes are reported. Even this small number
 415 of volcanoes, locally, leads to an increase in the already positive MNMB. Thus, globally, the average MNMB is higher in CARNALTI than in REF.

Concerning the fractional gross error (FGE), changes are also located in the vicinity of volcanoes (see Fig. S6). In those areas, especially in Central Africa and in Indonesia, the FGE is reduced from a maximum of 1.2 in REF to a maximum of 0.6

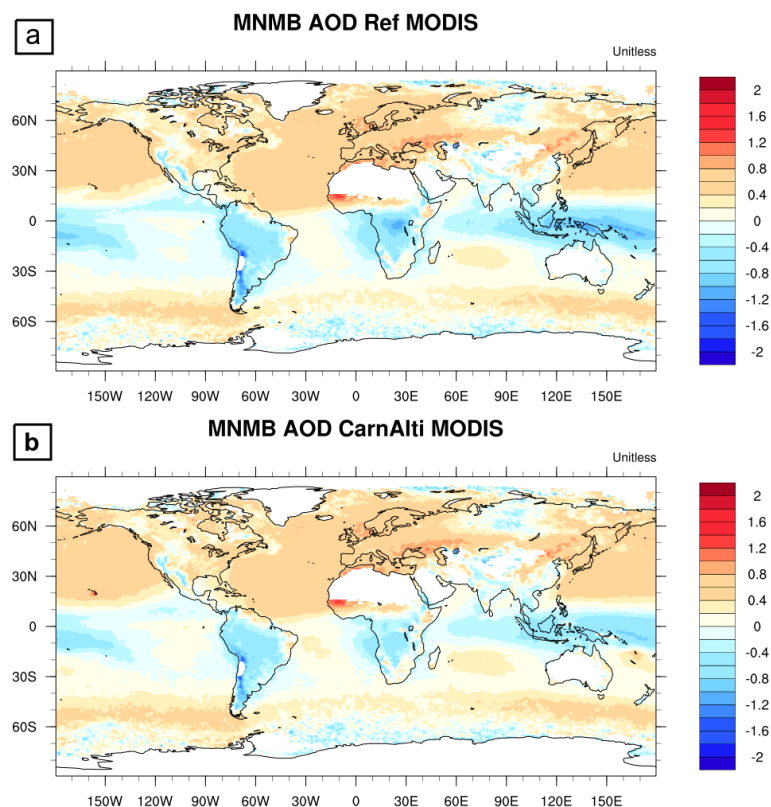


Figure 5. Maps of the 2013 annual MNMB of aerosol optical depth against MODIS monthly observations for (a) REF and (b) CARNALTI simulations.

in CARNALTI. Globally, the FGE score is slightly improved; 0.44 for REF and 0.43 in CARNALTI. Even if, locally in the
 420 Northern Hemisphere (*e.g.* in Hawaiï), the FGE score can be deteriorated in the simulation with Carn et al. (2016, 2017), at the
 global scale, with the new inventory is better.

The correlation coefficient R score is better in the Northern Hemisphere (see Fig. S6). Therefore, by adding new volcano
 point sources, and mostly in the Southern Hemisphere, the scores are higher in CARNALTI. The lifetime of aerosols increases
 when located in higher altitude. Aerosols are better represented in the CARNALTI simulation thanks to the use of a better
 425 injection altitude of SO_2 (precursor of sulfate aerosols contributing to the AOD).

By using Carn et al. (2017), the model results are improved in Zone 1. The MNMB raises from -0.53 with REF simulation
 to -0.28 in CARNALTI run. Similarly, the FGE and correlation coefficient are improved. In Fig. 6 (left column for Zone 1),
 the negative MNMB score in the REF simulation highlights the lack of the Nyamuragira volcanic SO_2 emissions. MNMB is
 largely reduced in CARNALTI simulation.

430 In Zone 2, unlike the previous area, the MNMB is already positive. Thus, by adding more SO_2 volcanic emissions, it
 increases the sulfate aerosol content leading to a deterioration of the MNMB and FGE scores (Table 3). The correlation

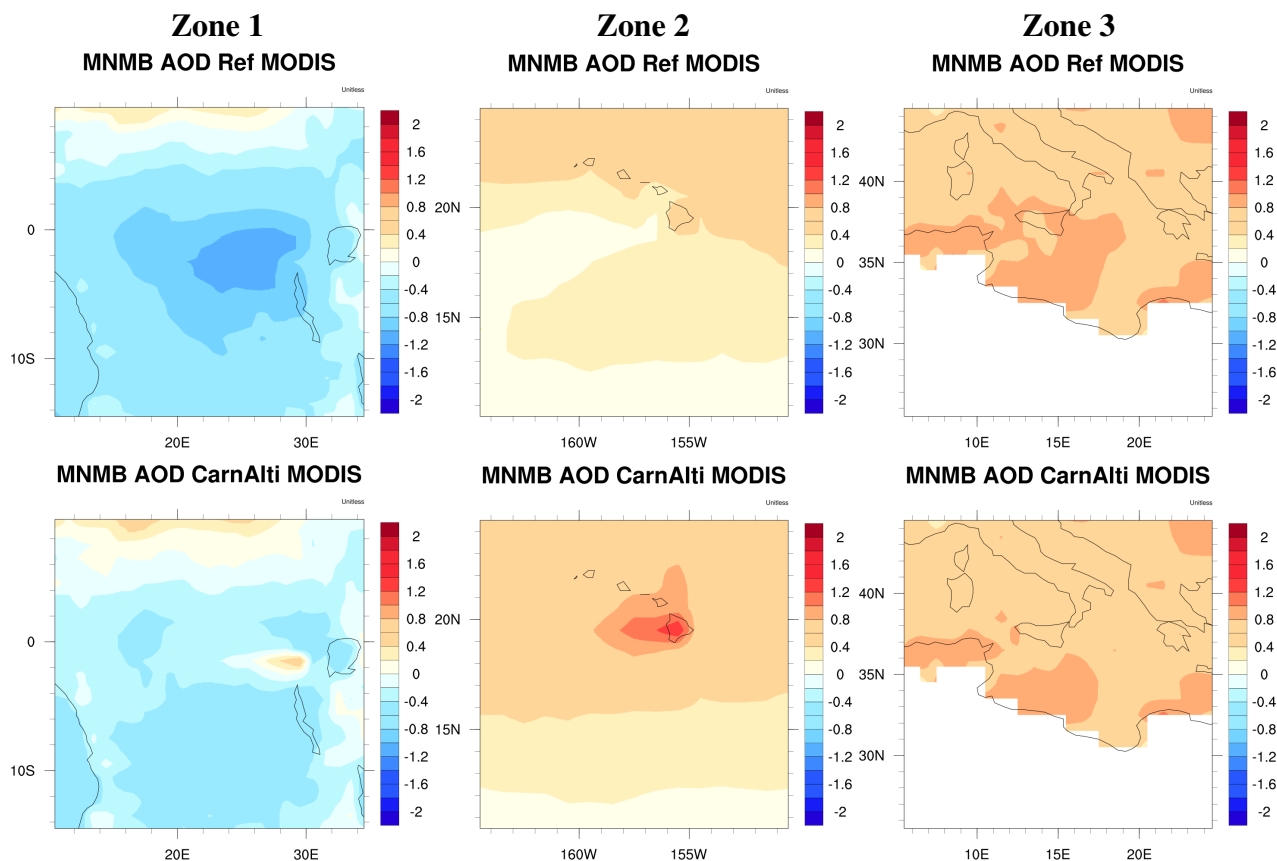


Figure 6. Maps of the 2013 annual MNMB of REF and CARNALTI simulations against MODIS observations at the specific zones.

coefficient increases due to a more accurate altitude where the emissions are injected in the CARNALTI simulation. Figure 6 in the middle column confirms these results. However, with the volcano being located at an altitude of 1222 m, where the sensitivity of infra-red, mostly, but also ultra-violet instruments is reduced, the estimation in the inventory for this volcano may be over-estimated.

In Zone 3, the statistical scores are almost similar for the two simulations. Indeed, in this region there are various other aerosols sources (industries, transport, dust,...) and sulfate from volcanic emissions do not dominate. Still, we can see in Fig. 6 a small improvement of MNMB between REF and CARNALTI simulations. The FGE and correlation scores are also a bit better in CARNALTI. Thus, using Carn et al. (2016, 2017) and injecting volcanic emissions at the actual altitude of the volcanoes slightly enhances MOCAGE performances.

5.3 Summary of the evaluation

The evaluation of MOCAGE performances against OMI SO₂ total column and MODIS AOD, shows an improvement of CARNALTI simulation compared to REF. The previous inventory [Andres and Kasgnoc (1998)] lacks some volcanic sources

Table 4. Global and local (Zones 1, 2 and 3) 2013 annual mean concentrations in REF, CARN and CARNALTI simulations. Gases are in mol and aerosols in kg.

		<i>Mean Tropospheric Column</i>			<i>Mean Surface Concentration</i>		
		SO ₂ (mol m ⁻²)	Sulfate (kg m ⁻²)	PM _{2.5} (kg m ⁻²)	SO ₂ (mol m ⁻³)	Sulfate (kg m ⁻³)	PM _{2.5} (kg m ⁻³)
Global	REF	7.51e-6	3.25e-6	5.75e-5	7.18e-9	5.65e-10	1.26e-8
	CARN	7.92e-6	3.52e-6	5.78e-5	8.21e-9	5.91e-10	1.27e-8
	CARNALTI	8.27e-6	4.01e-6	5.85e-5	7.23e-9	5.88e-10	1.27e-8
Zone 1	REF	7.84e-6	3.93e-6	5.44e-5	4.86e-9	5.37e-10	6.03e-9
	CARN	1.28e-5	7.06e-6	5.88e-5	9.06e-9	7.51e-10	6.35e-9
	CARNALTI	1.28e-5	1.12e-5	6.51e-5	4.84e-9	1.01e-9	6.85e-9
Zone 2	REF	4.13e-6	4.43e-6	7.10e-5	4.42e-9	3.75e-10	2.27e-8
	CARN	1.45e-5	8.03e-6	7.37e-5	1.77e-8	1.11e-9	2.33e-8
	CARNALTI	2.25e-5	1.31e-5	7.92e-5	2.74e-9	1.21e-9	2.34e-8
Zone 3	REF	4.74e-5	7.66e-6	2.443e-4	4.39e-8	1.67e-9	4.75e-8
	CARN	3.22e-5	6.63e-6	2.419e-4	3.03e-8	1.25e-9	4.83e-8
	CARNALTI	3.13e-5	6.84e-6	2.424e-4	2.30e-8	1.07e-9	4.81e-8

which leads to a global underestimation of sulfur dioxide concentrations and aerosol concentrations in the tropics (e.g. in
445 Zone 1). With the new inventory [Carn et al. (2016, 2017)] used in the CARNALTI simulation, volcanic emissions are larger.
Even if in some areas the scores are deteriorated, e.g. in Zone 2 where the model is already overestimating aerosol concentra-
tions, the scores at the global scale and in the vicinity of most of the volcanoes are improved.

6 Impact of the volcanic emission inventory update on the species concentration

SO₂, sulfate aerosols and PM_{2.5} tropospheric column and surface concentrations are summarized in Table 4. In order to disso-
450ciate the effect of the quantity of SO₂ emitted and of the injection altitude, we compare the REF and CARNALTI simulations
with the CARN run. The annual mean sulfur dioxide total column, at the global scale, is 8.27e-6 mol m⁻² in the CARNALTI
simulation, 10 % higher to the 7.51e-6 mol m⁻² in REF. Regarding aerosols species, sulfate total column is 23 % higher in the
CARNALTI simulation but only by 2 % for PM_{2.5}, because it is only partially composed of sulfate. This increase is explained
by the greater amount of SO₂ emitted in Carn et al. (2016, 2017) and by the new injection configuration. At higher altitudes, the
455 lifetime of sulfur species is longer due to slower removal processes [Stevenson et al. (2003)]. Figure 7 illustrates this concept.
It shows the relative difference of sulfate tropospheric column between CARNALTI and REF experiments. We clearly see an
increase in CARNALTI concentrations in the vicinity of most volcanic point sources.

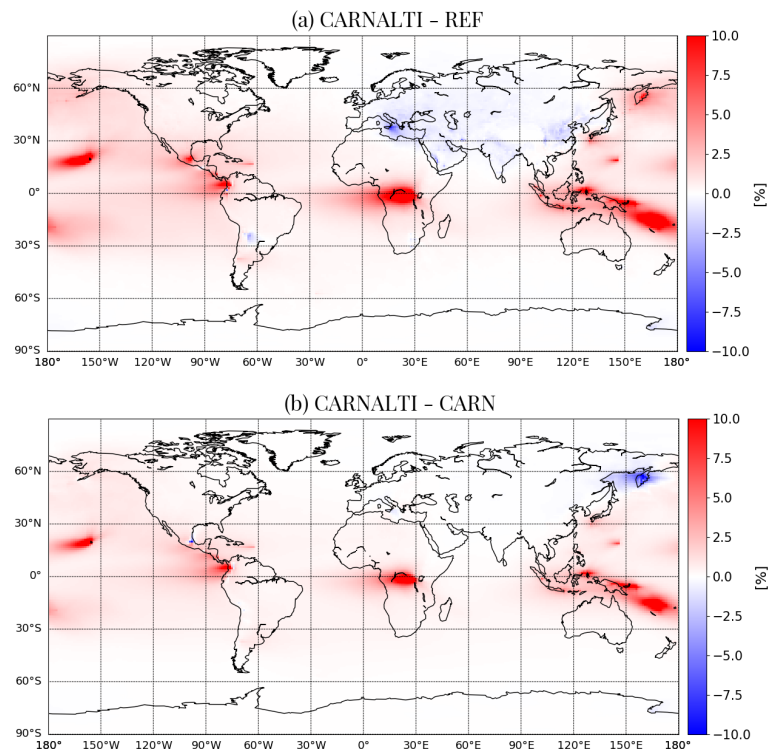


Figure 7. 2013 annual mean sulfate tropospheric column relative difference between the (a) CARNALTI and REF simulations and (b) CARNALTI and CARN simulations, in %.

Surface concentrations, at the global scale, from the simulations show different results. The sulfur species' concentrations still increase but by less; from $5.65\text{e-}10 \text{ kg m}^{-3}$ in REF simulation to $5.88\text{e-}10 \text{ kg m}^{-3}$ (5 %) in CARNALTI for sulfate and from $7.18\text{e-}9 \text{ mol m}^{-3}$ to $7.23\text{e-}9 \text{ mol m}^{-3}$ (<1 %) for SO_2 . In the CARN simulation results, where the volcanic emissions are injected at the model surface, we notice higher concentrations of all sulfur species at the surface. SO_2 and sulfate concentrations are $8.21\text{e-}9 \text{ mol m}^{-3}$ and $5.91\text{e-}10 \text{ kg m}^{-3}$ respectively, being around 6 % higher for each species compared with REF but 12 % higher, for SO_2 , against the CARNALTI simulation. Thus, by injecting volcanic emission higher in altitude with the new configuration in the CARNALTI simulation, less sulfur species remain at the surface and therefore aerosols are spread further from the volcanoes (see Fig. 7b, where we can see volcanic plumes 150 to 200 km away from their source location).

By looking at the local scale, the differences between CARNALTI and REF can be very large. For example, in Zone 2, the SO_2 tropospheric column is 5 times larger in CARNALTI (from $4.13\text{e-}6$ in REF to $2.25\text{e-}5 \text{ mol m}^{-2}$), 3 times larger for the aerosol sulfate total column (from $4.43\text{e-}6$ to $1.31\text{e-}5 \text{ kg m}^{-2}$) and 3 times larger for sulfate at the surface ($3.75\text{e-}10$ to $1.21\text{e-}9 \text{ kg m}^{-3}$). In Zone 1, changes are also more important compared to the global scale, with 63 % more concentration of SO_2 and 185 % higher concentration of sulfate in the atmosphere and 88 % more sulfate at the surface. In Zone 3, there is less impact because it is a more polluted area.

The difference between CARN and CARNALTI SO₂ and aerosol sulfate tropospheric columns are not as important as between REF and CARNALTI. Sulfur species concentrations are highest in CARNALTI, with the exception of SO₂ in Zone 3. In this highly polluted area, anthropogenic emissions are dominant. The volcanic SO₂ emitted is then more likely to compete with SO₂ from other sources leading to an increase of its lifetime. At the surface, as expected, the SO₂ concentration is much higher in all zones in CARN simulation compared to CARNALTI (e.g. 85 % smaller in Zone 2 in CARNALTI compared to CARN). However, for sulfate aerosols, the surface concentrations are higher in CARNALTI run compared to CARN in Zone 1 and Zone 2. With volcanic emissions injected into the upper levels of the model, the lifetime of SO₂ increases and more sulfate aerosols are formed (as we can see in the tropospheric column) and more is found sulfate near the surface.

Concerning particulate matter, the impact of Carn et al. (2016, 2017) at the global scale does not present significant changes (both in the tropospheric column and at the surface), because PM_{2.5} is not composed only of sulfate aerosols but are the sum of all the atmospheric aerosols with a diameter less than 2.5 μm. However, we found larger changes locally; e.g., 20 % higher PM_{2.5} tropospheric column concentration in CARNALTI with 6.51e-5 kg m⁻² compared to REF with 5.44e-5 kg m⁻², in Zone 1. As expected, for Zone 3, all chemical species concentrations are smaller in CARNALTI compared to REF simulation, especially at the surface.

7 MOCAGE sulfur budget

In this section, we calculate the MOCAGE sulfur budget and analyse the impact of the new volcanic SO₂ emissions on the tropospheric species distribution with the CARNALTI run. In order to isolate the contribution of volcanic emission from the other species concentration, we look at the difference between CARNALTI and NOVOLC simulations. The relative contribution of volcanic SO₂ emissions to the species budget is defined by the quantity of species in the CARNALTI simulation subtracted from the quantity of species in the NOVOLC simulation, with respect to the total quantity of species in the CARNALTI simulation:

$$Contribution_X = 100 \frac{X_{CARNALTI} - X_{NOVOLC}}{X_{CARNALTI}} \quad (5)$$

with $X_{CARNALTI}$ and X_{NOVOLC} the annual mean concentration of the parameter X in CARNALTI and NOVOLC simulations, respectively.

Hereafter, the parameters from NOVOLC simulation will be named "non-volcanic" parameters. On the contrary, "volcanic" parameters correspond to the parameters of CARNALTI simulation minus the quantity in the NOVOLC simulation. The CARNALTI simulation represents the total (volcanic + non-volcanic) concentration of the parameters.

7.1 Global budgets

The global sulfur budget simulated in CARNALTI is shown in Table 5. Annually and globally averaged SO₂ emissions, SO₂ and sulfate aerosols burdens as well as sulfur wet and dry depositions are used to calculate the sulfur budget.

Table 5. 2013 annual global mean SO₂ emissions, sulfur budget and deposition quantities in Tg. The contribution of sulfur species due to volcanic emissions or other emission sources are presented, in %. The efficiency is the ratio between the contribution of the sulfate burden and the contribution of the total sulfur emission attributed to a specific source. In other words, it is the fractional contribution from anthropogenic and volcanic sources to the sulfate burden.

	Sulfur	SO ₂	Sulfate	Sulfur Deposition			Efficiency
	Emission	Burden	Burden	Wet	Dry	Sedim	
Total (Tg)	81.41	0.17	0.82	42.41	27.81	9.80	-
<i>Sources contributions to the total budget (%)</i>							
Volcanoes	14.5	13.8	27.4	7.9	2.3	23.0	1.89
Other	85.5	86.2	72.6	92.1	97.7	77.0	0.85

Volcanic emissions are of 11.8 Tg/yr. This estimation remains in the range of previous studies which estimated volcanic emissions between 7 Tg and 14 Tg [Berresheim and Jaeschke (1983), Chin and Jacob (1996), Graf et al. (1997), Sheng et al. (2015) updated in Feinberg et al. (2019)]. However, due to lower anthropogenic emissions compared to those studies because of the recent year chosen (2013), the 15% contribution from volcanic emissions to the total sulfur emissions in CARNALTI is higher.

The global SO₂ burden is 0.17 Tg, slightly smaller than but closer to other studies whose values range from 0.2 Tg to 0.52 Tg [Pham et al. (1995), Chin and Jacob (1996), Feichter et al. (1996), Graf et al. (1997), Stevenson et al. (2003), Feinberg et al. (2019)]. Stevenson et al. (2003) explained that the SO₂ burden in a simulation can change depending on the distribution of oxidants and the deposition scheme used in the models. Moreover, those studies were done on earlier periods of time when anthropogenic SO₂ emissions were superior compared to 2013 in our simulation. In our simulation, 21.97 Tg S are directly removed by dry and wet deposition of sulfur dioxide, representing a percentage of almost 27 %. Thus, the transformation rate of SO₂ to sulfate is about 73 %; a bit higher but consistent with the studies reported above (from 50 to 66 %).

The global vertical sulfate column is 0.82 Tg S, comparable with other studies; 0.53 Tg S in Chin and Jacob (1996), 0.78 Tg S in Graf et al. (1997), 0.81 Tg S in Stevenson et al. (2003) and 0.64 Tg S in Feinberg et al. (2019).

These results confirm the non-linear contribution of the different SO₂ sources emissions to the sulfate burden. Indeed, volcanic sources represent almost 15 % of the total SO₂ emitted into the atmosphere, but they contribute 27 % to the sulfate burden. The transformation of SO₂ into sulfate from the other sources is not as efficient. We can note a higher efficiency for the volcanic sources, around 1.89, compared to the other sources, 0.85.

The total sulfur deposition is 80 Tg S, including 22 Tg S of SO₂, a little less than the total sulfur deposition in Feinberg et al. (2019), of 94 Tg S also including 22 Tg S of SO₂. The difference comes from the aerosol deposition, which depends on the deposition scheme and the meteorological fields which can vary depending on the considered time period. In our study, the sulfur deposition is mainly wet deposition. Precisely, the partition of each deposition fluxes are 52 % for wet deposition, 35 % for dry deposition and 12 % from sedimentation. But, sulfur deposition due to volcanic emissions is weaker than for the other sources: 8 % for wet deposition, 23 % for sulfate aerosol sedimentation and only 2 % for dry deposition. Due to the

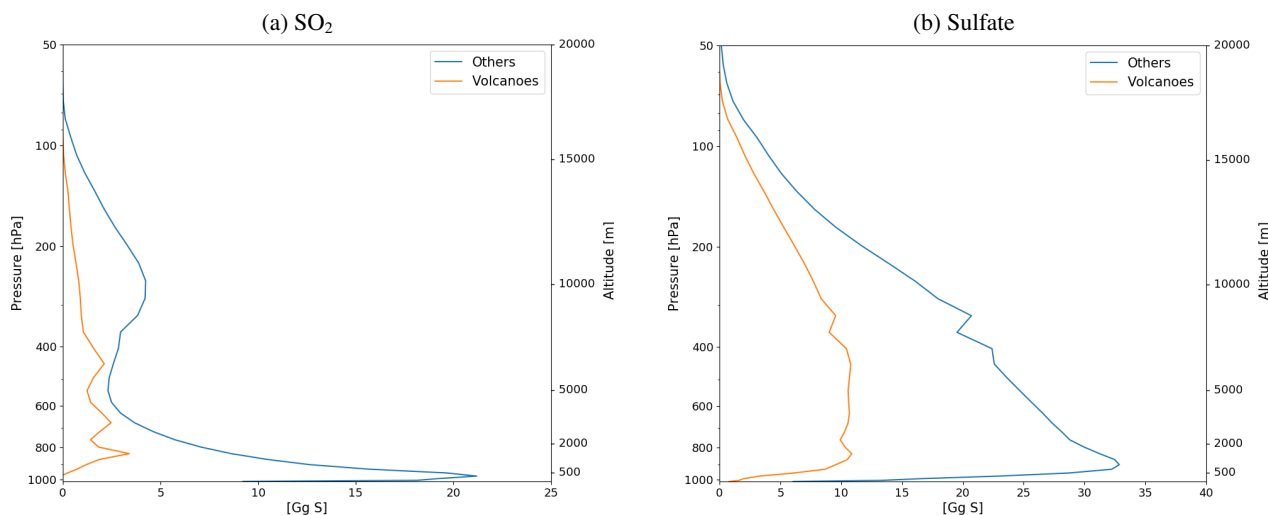


Figure 8. 2013 annual global mean vertical profile for (a) SO_2 and (b) sulfate aerosols from volcanic and other sources.

higher altitude of injection, the atmospheric residence time for volcanic sulfur species is longer and the deposition rate lower, especially for the dry deposition.

7.2 Vertical distribution

Figure 8 shows the global and annually averaged vertical profiles for sulfur dioxide and sulfate concentrations for 2013.

530 Anthropogenic and volcanic sources are separated to highlight the main differences between them.

Non-volcanic SO_2 dominates the entire vertical column, with a maximum at the surface linked to anthropogenic emissions, emitted at the model surface. On the contrary, the vertical distribution from volcanic SO_2 shows variations. **There is no contribution below 950 hPa but there are three maxima above; one at 850 hPa (about 1500 m) due mostly to passive degassing, another around 680 hPa (about 3300 m) due to passive degassing from high-altitude volcanoes and eruptions, and the last one**
 535 **around 450 hPa (about 6000 m) due to high-altitude eruptions. It is noteworthy that even with few eruptive events during the year 2013, the volcanic SO_2 vertical distribution is affected by them.**

Concerning sulfate aerosols, volcanic emissions are also not dominant over the entire vertical column. Non-volcanic sulfate aerosol have the highest values around 950 hPa, near the surface. For volcanic sulfate, the maximum is between 850 and 450 hPa but four times smaller than for other sources and without any specific peak associated to passive degassing or eruptive
 540 emissions. These results are different from Graf et al. (1997), which shows that the vertical distribution of volcanic sulfate aerosols is comparable to anthropogenic and biomass burning sulfate and is even dominant between 800 and 300 hPa (the altitude of volcanic emissions, mainly from eruption). **This difference between our study and Graf et al. (1997) can be explained by the quantity of SO_2 emitted by eruptions. In 2013, only a few eruptive events occurred while almost 30% of volcanic emissions in Graf et al. (1997) are eruptive. Therefore, with a greater amount of volcanic emissions injected at higher altitude**

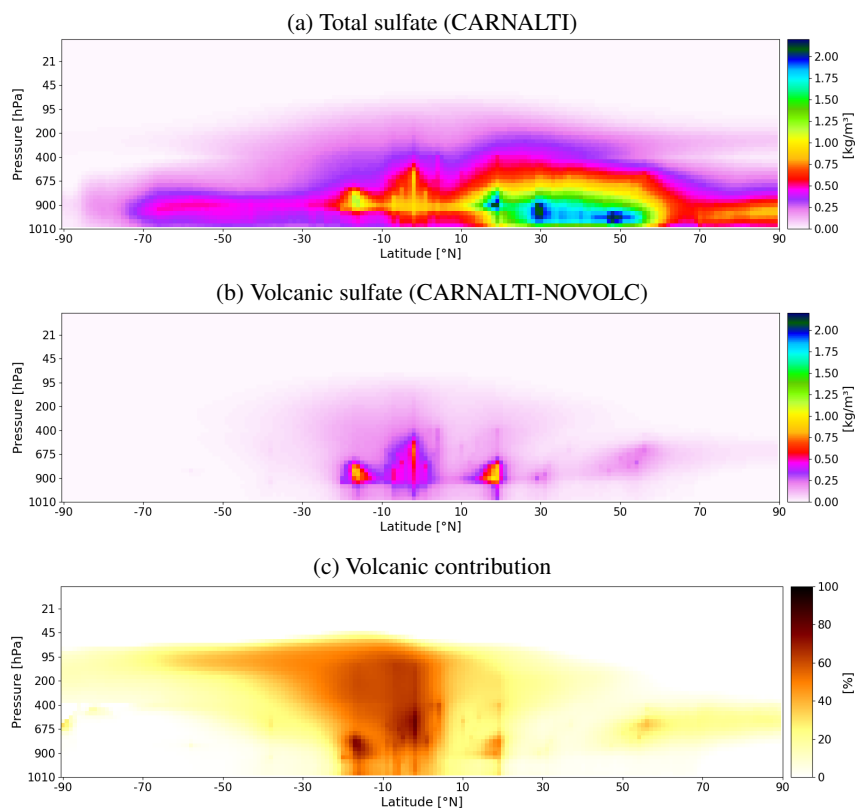


Figure 9. 2013 annual zonal mean (a) total sulfate concentration (in kg m^{-3}), (b) volcanic sulfate concentration (in kg m^{-3}) and (c) volcanic sulfate contribution (in %).

545 in Graf et al. (1997), the potential to form sulfate aerosols is greater than in our study. This can explain the greater efficiency
of 2.63 in the tropospheric sulfate burden in Graf et al. (1997) compared to 1.89 in our study.

Figure 9a represents the annual zonal mean sulfate concentration. Most of the sulfate aerosols reside in the Northern Hemisphere (between 15°N and 55°N) due to anthropogenic influence and the highest values are below 900 hPa (close to the surface). The sulfate concentrations due to volcanic emissions (Fig. 9b) are located at higher altitudes. On both sides of the
550 equator, volcanic sulfate is found between 900 and 650 hPa. Over the tropical region, the volcanoes contribution to the sulfate aerosol concentrations is larger, with a maximum of 75-80 % around 650 hPa (see Fig. 9c). We also notice that sulfate aerosols are transported by the general atmospheric circulation, up to the UTLS (Upper Troposphere - Lower Stratosphere) and from the equator to the poles, especially in the Southern Hemisphere where there are more volcanoes.

7.3 Regional distributions

555 The volcanic contribution to the global surface SO_2 concentrations is relatively low, around 14 %, but it is much higher close to the source points (see Fig. 10, top for SO_2). This is mainly due to the high altitude of emissions from volcanoes. Similarly,

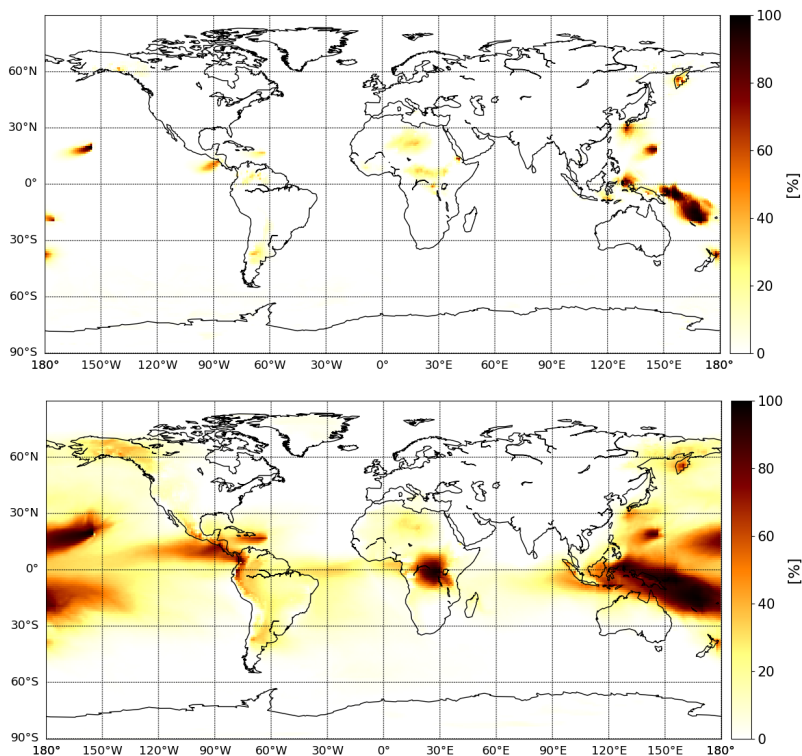


Figure 10. 2013 annual mean (top) SO_2 and (bottom) sulfate surface contribution due to volcanic emission (in %).

Fig. 10 (bottom for sulfate aerosol) shows a greater influence of volcanic emissions on the sulfate aerosol concentration at the surface, almost larger than other sources in the vicinity of volcanoes. Globally, the mean contribution is of 19 %, but with a rather low, almost zero, contribution over continental areas in the Northern Hemisphere. Considering that within the boundary layer, anthropogenic SO_2 emissions are dominant, the sulfate aerosols formed in this environment come largely from anthropogenic rather than from other sources. However, in areas with small anthropogenic sources (Indonesia, Hawaiï and Central Africa), the volcanic contribution is large.

For the total column, volcanic emissions contribute much to the sulfur species burden; 24 % to SO_2 and 21 % to sulfate aerosols. In Fig. 11, we can see that the highest sulfate burden is located over polluted areas (East of North America, Europe, Middle-East, India and China) as well as near some volcanoes and particularly over oceanic volcanoes. By looking at the volcanic contribution, we note that the sulfate aerosols due to volcanic emissions are mainly distributed over the oceanic environment in the tropics (also corresponding to volcanoes of lower altitudes). The highest contribution, 85 %, is found over Indonesia.

The annual global depositions of sulfur species due to volcanic emissions are 20 %, 5 % and 26 % for wet deposition, dry deposition and sedimentation, respectively. Figure 12 represents the total sulfur deposition at the global scale and shows higher deposition fluxes over anthropogenic polluted areas, where volcanic contribution is low (see Fig. 12b). The only exception

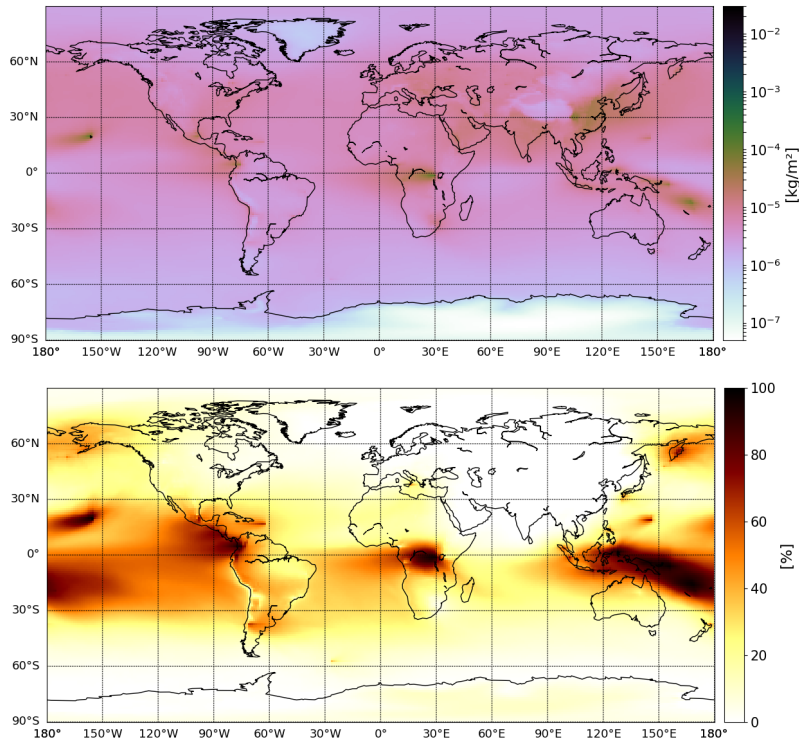


Figure 11. (top) 2013 annual mean sulfate tropospheric column from CARNALTI (in kg m^{-2}) and (bottom) its contribution due to volcanic emissions (in %).

where there are a high deposition flux and a high volcanic contribution is Indonesia. Details on the proportion of each type of deposition (wet, dry and sedimentation) are shown in Fig. S10, where we notice a weak influence of sedimentation, consistent with Table 5, compared to wet and dry depositions.

575 8 Sensitivity analysis on passive volcanic sources

Carn et al. (2017) provide for passive degassing not only the annual SO_2 volcanic emissions ($\overline{E_{V,Y}}$, V=volcano, Y=year), but also the associated annual emission uncertainties ($U_{V,Y}$) for each volcanic source. Thus, in this section, we aim at using this information to check the variability induced in MOCAGE sulfur budget and to analyse how it affects our conclusions from the previous section.

580 8.1 Description of the supplementary simulations

Three additional simulations are conducted to analyse the sensitivity of the MOCAGE model to the uncertainty of volcanic passive emissions. The first one, named CA_MIN, takes into account for each volcano the lowest estimation of SO_2 emissions. In

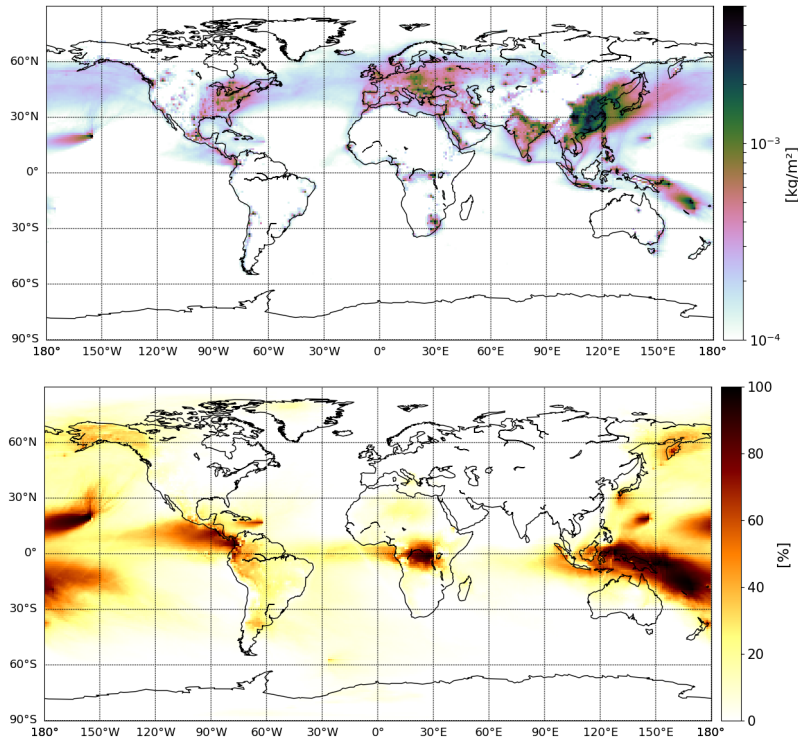


Figure 12. (top) 2013 annual mean sulfur deposition from CARNALTI (in kg m^{-2}) and (bottom) its contribution due to volcanic emissions (in %).

other words, for each volcano, we remove the annual emission uncertainty to the annual mean emission: $E_{V,Y} = \overline{E_{V,Y}} - U_{V,Y}$. In contrast, the second simulation, named CA_MAX, takes into account the highest estimation of SO_2 emission; we add the
 585 annual emission uncertainty to the annual mean emission: $E_{V,Y} = \overline{E_{V,Y}} + U_{V,Y}$. Thus, both CA_MIN and CA_MAX experiments do not have daily variations due to passive degassing, but only due to eruptions. For the last one, named CA_RAND, emissions are randomly determined on a daily basis within the annual emission uncertainty interval $[\overline{E_{V,Y}} - U_{V,Y}, \overline{E_{V,Y}} + U_{V,Y}]$ following a continuous uniform distribution. Thus, daily variations are not only due to eruptions but also to passive degassing, as expected in reality. The reference simulation used, CARNALTI, is called CA from now on.

590 Figure 13 presents the 2013 temporal evolution of SO_2 total emission for each simulation. As in Fig. 1, we note the annual variation due to anthropogenic emissions, representing a common basis of around 70 Tg S yr^{-1} for all simulations, as well as the daily variation due to eruptions, shown by the large peaks and representing a value of 0.10 Tg S in 2013. Therefore, the differences are only due to passive degassing SO_2 emissions. In the CA simulation, the annual total passive degassing emission is 11.74 Tg S . In the CA_MIN, CA_MAX and CA_RAND experiments, it is 10.60 , 12.95 and 11.75 Tg S , respectively.
 595 Thus, there is a relative difference of 10.6% with respect to the annual mean volcanic emissions for CA_MIN simulation but a difference of 1.4% when considering all sulfur emissions. Similarly, volcanic emissions in CA_MAX and CA_RAND

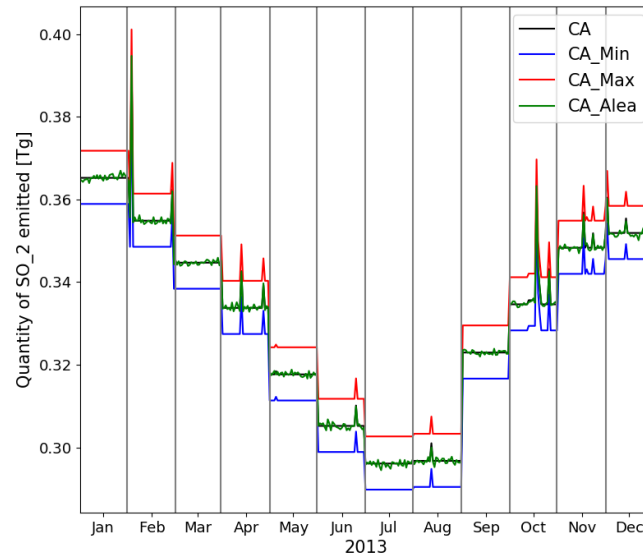


Figure 13. Temporal evolution of 2013 SO_2 emissions, corresponding to CA (black), CA_MIN (blue), CA_MAX (red) and CA_RAND (green) simulations.

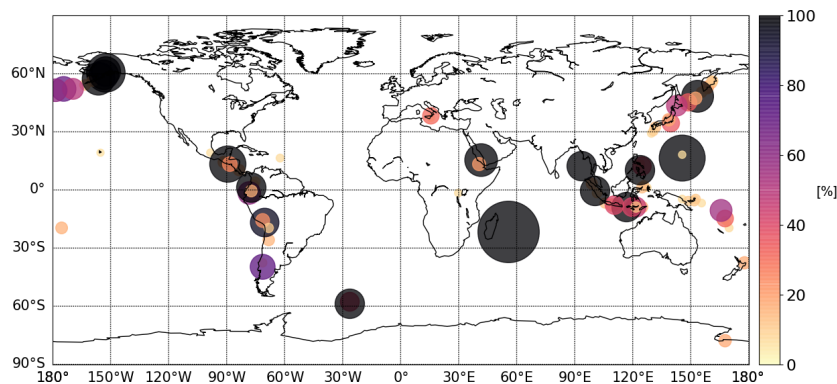


Figure 14. Map of $U_{V,Y} = \overline{E_{V,Y}}$ ratio of SO_2 emissions (in %) in Carn et al. (2017). The size of the circles is proportional to the value of the ratio, also represented by the color.

simulations are 9.3 % and 0.1 % higher than in CA, which represents a difference of 1.5 % and < 0.01 % respectively with respect to the total sulfur emissions.

We expect a greater sensitivity to the annual emission uncertainty at volcanoes where the proportion of the annual uncertainty with respect to the annual mean emission is close to 100 %. Figure 14 represents the percentage of uncertainty on the annual measurement of volcanic emission per volcano in Carn et al. (2017). The darker and bigger the circle is, the more important is the uncertainty compared to the mean emission.

Table 6. As in Table 5 but for CA_MIN, CA_MAX and CA_RANDOM simulations.

		Sulfur	SO ₂	Sulfate	Sulfur Deposition			Efficiency
		Emission	Burden	Burden	Wet	Dry	Sedim	
CA_MIN	Total	80.27	0.16	0.80	41.45	28.14	10.01	-
	<i>Sources contributions to the total budget (%)</i>							
	Volcanoes	13.33	12.68	25.30	5.74	3.43	24.59	1.90
	Other	86.67	87.32	74.70	94.26	96.57	75.41	0.86
CA_MAX	Total	82.62	0.17	0.84	42.75	28.38	10.48	-
	<i>Sources contributions to the total budget (%)</i>							
	Volcanoes	15.80	14.87	29.02	8.61	4.27	28.01	1.84
	Other	84.20	85.13	70.98	91.39	95.73	71.99	0.84
CA_RANDOM	Total	81.42	0.17	0.82	42.09	28.26	10.24	-
	<i>Sources contributions to the total budget (%)</i>							
	Volcanoes	14.55	13.74	27.17	7.17	3.83	26.30	1.87
	Other	85.45	86.26	72.83	92.83	96.17	73.70	0.85

8.2 Sensitivity study on the global budget in MOCAGE

As in Table 5 for CA, Table 6 presents the annual mean global sulfur budget for the CA_MIN, CA_MAX and CA_RANDOM simulations. Even if the total sulfur species burdens are similar in all simulations with SO₂ burden around 0.17 Tg S and sulfate burden between 0.80-0.84 Tg S, the contribution of the volcanic emissions to the total budget varies. In the CA experiment, the volcanic contribution to the sulfate aerosol burden is 27.40 %, but it ranges from 25.30 % in the CA_MIN experiment to 29.02 % in the CA_MAX experiment. This implies a variation in the efficiency of the model MOCAGE to produce sulfate aerosols from volcanic SO₂ emissions. The greatest efficiency score is 1.90 for the CA_MIN simulation, meaning that smaller amounts of SO₂ emitted can form sulfate more efficiently. This illustrates the non-linear relationship between the volcanic SO₂ emission and the sulfur budget.

Figures 15 illustrate the spatial difference in volcanic SO₂ contribution between CA and CA_MIN, CA_MAX and CA_RANDOM. The differences with CA_MIN or CA_MAX (Fig. 15a and 15b) are similar but of opposite sign. As expected, differences are located in the vicinity of volcanic point sources but especially near volcanoes with a high $U_{V,Y}/\overline{E_{V,Y}}$ ratio (see Fig. 14).

The contribution of volcanic SO₂ to the SO₂ burden is larger (less important resp.) in the CA_MAX simulation with 14.87% (the CA_MIN simulation resp. with 12.68%) than in the CA simulation with 13.80%. The difference between CA and CA_RANDOM are weaker. Daily variations in SO₂ emissions of volcanoes (CA_RANDOM) do not change significantly the annual mean contribution of volcanic SO₂ tropospheric column. The same conclusions are shown in Fig. S6 for the sulfate tropospheric column.

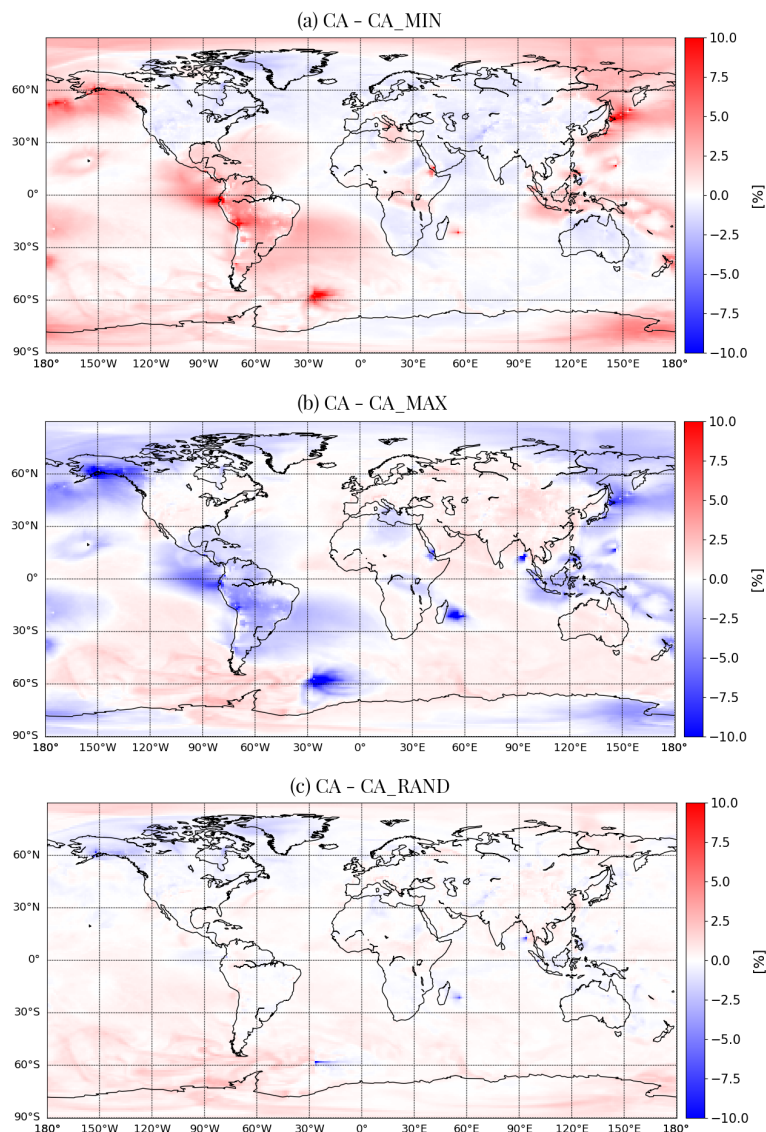


Figure 15. 2013 annual mean difference in SO_2 tropospheric column volcanic contribution between CA and (a) CA_MIN, (b) CA_MAX and (c) CA_RAND simulations, in %.

620 The differences between the simulations are mostly in the deposition fluxes. Regardless of the sensitivity simulation, the sulfur deposition by dry deposition or sedimentation is higher than in the CA simulation. As an example, the sulfur sedimentation is 9.80 Tg in the CA simulation but 10.01, 10.48 and 10.24 Tg in the CA_MIN, CA_MAX and CA_RAND simulations, respectively. It represents a contribution of 22.97 % for CA and 24.59, 28.01 and 26.30 % for CA_MIN, CA_MAX and CA_RAND, respectively. Thus, sulfur deposition does not react linearly both to the quantities of volcanic SO_2 emitted (with respect to
 625 CA_MIN and CA_MAX simulations) and to the spatio-temporal variability of these emissions (with respect to CA_RAND).

Finally, in the CA_MAX experiment, with the highest estimation of volcanic emissions, we find, as expected, a higher sulfur burden as well as higher sulfur deposition quantities. However, the CA_MIN simulation assumes the lowest estimate of volcanic SO₂ emissions and gives only a slightly lower total sulfur deposition (79.60 Tg S compared to 80.02 Tg S in CA) but with a different partition. While wet deposition is lower between CA and CA_MIN, dry deposition and sedimentation are more important in the CA_MIN simulation. Even when applying a daily variation, with nearly the same total annual quantity of volcanic SO₂ emitted (the CA_RAND simulation), we notice changes in the MOCAGE sulfur budget.

9 Conclusions

In this paper, the aim was to study the contribution of volcanic sulfur emissions on the tropospheric composition and on sulfur species surface concentration and deposition, at the global scale. Previously, the volcanic emissions inventory implemented in MOCAGE was from Andres and Kasgnoc (1998), but it has become obsolete. Therefore, a new volcanic SO₂ emission inventory, based on Carn et al. (2016, 2017), is implemented in MOCAGE. Thanks to satellite technologies, used to compile this inventory, it includes more volcanoes and gathers both eruptive emissions and passive degassing at a fine time resolution compared to previous inventories. Eruptions are provided as daily total amounts and passive degassing as annual averages with associated annual uncertainties. The inventory also provides information on the plume altitudes. A configuration to inject volcanic emission with an umbrella vertical profile was implemented in the model.

The choice was made to consider the year 2013, when quantities of volcanic SO₂ from eruptions are the lowest in the new inventory and negligible in the yearly average. Thereby, the study is focused on passive degassing emissions. [Two simulations are used to assess the new version of MOCAGE using the Carn et al. \(2016, 2017\) emissions \(CARNALTI\) and associated emission heights with respect to the previous implementation based on Andres and Kasgnoc \(1998\) \(REF\).](#)

The comparison of the MOCAGE simulations against [OMI SO₂ total column and MODIS AOD](#) shows that the statistical scores of the model were improved in the CARNALTI simulation compared to REF, especially at the local scale near the volcanoes. [The global concentration of SO₂ in MOCAGE simulation is increased with the new inventory. This largely reduces the bias against OMI measurements and increases the correlation with the instrument. Compared to MODIS AOD, the underestimation in aerosol content in the tropics is also reduced.](#) Hence, well constraining volcanic emission sources in Chemistry-Transport Models (CTM) is necessary, in order to better represent the tropospheric composition. The comparison to the MODIS AOD provides a method for validating the model results that is independent of the OMI data, which we also use for validation but was also used to help estimate the Carn et al. (2016, 2017) emissions.

We showed that considering more volcanoes (both passive degassing and eruptive types) and using a configuration to inject volcanic emissions aloft allows MOCAGE to increase sulfur species concentrations in CARNALTI compared to REF. At the surface, sulfur species concentrations and depositions were also increased, especially in the vicinity of the volcanoes, affecting air quality in these areas.

Using this new volcanic emissions inventory, we calculated the model sulfur budget in the troposphere. It shows that even if volcanic emissions represents only 15 % of the total sulfur emissions, the contribution of volcanic SO₂ emissions to the sulfur

660 tropospheric burden is non-linear. Indeed, volcanic sulfate burden is around 27 %, pointing out that the volcanoes efficiency to the sulfur budget is greater than from other sources. Similarly, sulfur deposition due to volcanic emissions contributes unequally to the total sulfur deposition, depending on the nature of deposition; e.g. volcanic sulfate aerosols sedimentation represents the smallest proportion of the total volcanic sulfur deposition (about 12 %), but contributes significantly to the total sulfur sedimentation from all types of SO₂ sources (about 23 %).

665 Moreover, the sensitivity study shows that by increasing, decreasing or including temporal variations in volcanic emission fluxes, the global sulfur budget changes non-linearly. As an example, despite a reduction in the amount of volcanic SO₂ emitted in CA_MIN, the distribution in sulfur deposition varies, causing the decrease of wet deposition but the increase of dry deposition and sedimentation compared to CARNALTI.

670 These results show that the Carn et al. (2016, 2017) inventory brings an improvement in volcanic SO₂ emissions at the global scale. However, there are still remaining uncertainties. Even if recent important progress was made in SO₂ remote sensing, there are various uncertainties in SO₂ retrievals from satellites of emission mass and height (for eruptions) (e.g., vertical sensitivity of the instruments, limits of detection, assumptions in the retrieval algorithm, spatial coverage, data gaps due to clouds, . . .) and in the methods used to derive the volcanic emissions from these retrievals. With the constant improvements of space-borne instruments and of methods, more and more accurate volcanic SO₂ inventories will be produced in the coming years. For example, TROPOMI instrument, with its high spatial resolution and higher-quality SO₂ dataset, could provide improved emission inventories [Theys et al. (2019), Fioletov et al. (2020)] and could also be used to validate model in similar study as this one, but in more recent year (2018 and later). Further gains could also be made by increasing the temporal coverage of the satellite observations, which would enable more frequent updating of the emission inventories associated with transient volcanic eruptions. However, this would either require more satellites to be launched into low Earth orbit or a geostationary satellite.

680 In this study, we focused on one particular year. By choosing the 2013 year, we mainly study the impact of passive degassing emissions. However, additional studies considering a year when volcanic eruptions were larger and more frequent would be complementary; e.g. in 2014, 5.35 Tg of eruptive emissions are referenced, almost thirty times more than in 2013. It would be interesting to compare and analyse the specific impact of eruptive emissions on the tropospheric sulfur budget. However, the comparison of the tropospheric sulfur budget between different years cannot only be affected by the differences in volcanic sulfur emissions. Indeed, sulfur dioxide is a soluble species and the meteorological parameters can also impact the tropospheric sulfur budget; e.g., differences in precipitation can lead to changes in the wet deposition fluxes. Thus, meteorological parameters should be taken into account to analyse the inter-annual differences.

690 Finally, it could also be interesting to not only compare two years of the Carn et al. (2016, 2017), but to fully study the inter-annual variability of volcanic sulfur emissions over a longer period. Since the data are fully available over a decade (2005-2015), this type of study would be possible.

Data availability. The new volcanic SO₂ inventory implemented is available for eruptive emissions on GES DISC archive (<https://doi.org/10.5067/MEASURES/SO2/DATA404>) and for passive degassing emissions on Carn et al. (2017) supplementary information (<https://doi.org/10.1038/srep44095>). Concerning data used for the validation, [OMI SO₂ total column data can be find on the NASA database GES DISC \(https://doi.org/10.5067/Aura/OMI/DATA2022\)](https://doi.org/10.5067/Aura/OMI/DATA2022). The previous volcanic SO₂ inventory is available upon request from the corresponding author.

Supplement. The supplement related to this article is available online at: ...

Author contributions. CL, JG and VM designed the study and the model experiments. Simulations were carried by CL with help from JG and MC. The paper was written by CL and reviewed, commented and edited by VM, JG , NT, PDH and PS. All authors approved the article.

Competing interests. The authors declare that they have no conflict of interest.

700 *Acknowledgements.* We would like to acknowledge the MODIS mission team and scientists for the production of the data used in this study. The authors also thank Université Paul Sabatier Toulouse III for funding Claire Lamotte's PhD and Météo-France for hosting it at the Centre National de Recherches Météorologiques.

References

- Aas, W., Mortier, A., Bowersox, V., Cherian, R., Faluvegi, G., Fagerli, H., Hand, J., Klimont, Z., Galy-Lacaux, C., Lehmann, C. M. B.,
705 Lund Myhre, C., Myhre, G., Olivie, D., Sato, K., Quaas, J., Rao, P. S. P., Schulz, M., Shindell, D., Skeie, R. B., Stein, A., Takemura, T.,
Tsyro, S., Vet, R., and Xu, X.: Global and regional trends of atmospheric sulfur, *Scientific Report*, 953, <https://doi.org/10.1038/s41598-018-37304-0>, 2019.
- Adams, P. J., Seinfeld, J. H., Koch, D., Mickley, L., and Jacob, D.: General circulation model assessment of direct radiative forcing by the sulfate-nitrate-ammonium-water inorganic aerosol system, *Journal of Geophysical Research*, 106, 1097–1111,
710 <https://doi.org/10.1029/2000JD900512>, 2001.
- Andreae, M. O.: The Biogeochemical Cycling of Sulfur and Nitrogen in the Remote Atmosphere, vol. 159 of *C: Mathematical and Physical Sciences*, chap. 1, pp. 5–25, D. Reidel Publishing Company, 1985.
- Andres, R. and Kasgnoc, A.: A time-averaged inventory of subaerial volcanic sulfur emissions, *Journal of Geophysical research*, 103, 25 251–
25 261, <https://doi.org/10.1029/98JD02091>, 1998.
- 715 Barré, J., Peuch, V.-H., Attié, J.-L., El Amraoui, L., Lahoz, W., Josse, B., Claeysman, M., and Nédélec, P.: Stratosphere-troposphere ozone
exchange from high resolution MLS ozone analyses, *Atmospheric Chemistry and Physics*, 12, 6129–6144, <https://doi.org/10.5194/acp-12-6129-2012>, 2012.
- Bechtold, P., Bazile, E., Guichard, F., Mascart, P., and Richard, E.: A mass-flux convection scheme for regional and global models, *Quarterly
Journal of the Royal Meteorological Society*, 127, 869–886, <https://doi.org/10.1002/qj.49712757309>, 2001.
- 720 Berresheim, H. and Jaeschke, W.: The contribution of volcanoes to the global atmospheric sulfur budget, *Journal of Geophysical Research*,
88, 3732–3740, 1983.
- Boichu, M., Chiapello, I., Brogniez, C., Péré, J.-C., Thieuleux, F., Torres, B., Blarel, L., Mortier, A., Podvin, T., Goloub, P., Söhne, N.,
Clarisse, L., Bauduin, S., Hendrick, F., Theys, N., Van Roozendaal, M., and Tanré, D.: Current challenges in modelling far-range air
pollution induced by the 2014-2015 Bárðarbunga fissure eruption (Iceland), *Atmospheric Chemistry and Physics*, 16, 10 831–10 845,
725 <https://doi.org/10.5194/acp-16-10831-2016>, 2016.
- Boichu, M., Favez, O., Riffault, V., Petit, J.-E., Zhang, Y., Brogniez, C., Sciare, J., Chiapello, I., Clarisse, L., Zhang, S., Pujol-Söhne, N.,
Tison, E., Delbarre, H., and Goloub, P.: Large-scale particulate air pollution and chemical fingerprint of volcanic sulfate aerosols from
the 2014-2015 Holuhraun flood lava eruption of Bárðarbunga volcano (Iceland), *Atmospheric Chemistry and Physics*, 19, 14 253–14 287,
<https://doi.org/10.5194/acp-19-14253-2019>, 2019.
- 730 Carboni, E., Grainger, R., Walker, J., Dudhia, A., and Siddans, R.: A new scheme for sulphur dioxide retrieval from IASI measure-
ments: application to the Eyjafjallajökull eruption of April and May 2010, *Atmospheric Chemistry and Physics*, 12, 11 417–11 434,
<https://doi.org/10.5194/acp-12-11417-2012>, 2012.
- Carn, S.: Multi-Satellite Volcanic Sulfur Dioxide L4 Long-Term Global Database V3, <https://doi.org/10.5067/MEASURES/SO2/DATA404>,
https://disc.gsfc.nasa.gov/datasets/MSVOLSO2L4_3/summary, accessed: [2019-02-07], 2019.
- 735 Carn, S., Krotkov, N., Yang, K., and Krueger, A.: Measuring global volcanic degassing with the Ozone Monitoring Instrument (OMI),
Geological Society, London, 380, 229–257, <https://doi.org/10.1144/SP380.12>, 2013.
- Carn, S., Clarisse, L., and Prata, A.: Multi-decadal satellite measurement of global volcanic degassing, *Journal of Volcanology and Geother-
mal Research*, 311, 99–134, <https://doi.org/10.1016/j.jvolgeores.2016.01.002>, 2016.

- Carn, S., Fioletov, V., McLinden, C., Li, C., and Krotkov, N.: A decade of global volcanic SO₂ emissions measured from space, *Scientific Reports*, 7, <https://doi.org/10.1038/srep44095>, 2017.
- 740 Chestnut, L.: Human Health Benefits From Sulfate Reductions Under Title IV of the 1990 Clean Air Act Amendments, Final Report, Tech. rep., U.S. EPA, Office of Atmospheric Programs, Acid Rain Division, 1995.
- Chin, M. and Jacob, D.: Anthropogenic and natural contributions to tropospheric sulfate: A global model analysis, *Journal of Geophysical Research*, 101, 18 691–18 699, <https://doi.org/10.1029/96JD01222>, 1996.
- 745 Chin, M., Rood, R. B., Lin, S.-J., Muller, J.-F., and Thompson, A. M.: Atmospheric sulfur cycle simulated in the global model GOCART: Model description and global properties, *Journal of Geophysical Research*, 105, 24 671–24 687, <https://doi.org/10.1029/2000JD900384>, 2000.
- Clarisse, L., Coheur, P.-F., Theys, N., Hurtmans, D., and Clerbaux, C.: The 2011 Nabro eruption, a SO₂ plume height analysis using IASI measurements, *Atmospheric Chemistry and Physics*, 14, 3095–3111, <https://doi.org/10.5194/acp-14-3095-2014>, 2014.
- 750 Colette, A., Favez, O., Meleux, F., Chiappini, L., Haeffelin, M., Y., M., Malherbe, L., Papin, A., Bessagnet, B., Menut, L., Leoz, E., and Rouïl, L.: Assessing in near real time the impact of April 2010 Eyjafjallajökull ash plume on air quality, *Atmospheric Environment*, 45, 1217–1221, <https://doi.org/10.1016/j.atmosenv.2010.09.064>, 2010.
- Courtier, P., Freydisier, C., Geleyn, J.-F., Rabier, F., and Rochas, M.: The ARPEGE project at Météo-France, in: ECMWF Workshop, 1991.
- Cussac, M., Marécal, V., Thouret, V., Josse, B., and Sauvage, B.: The impact of biomass burning on upper tropospheric carbon monoxide: A study using MOCAGE global model and IAGOS airborne data, *Atmospheric Chemistry and Physics*, 20, 9393–9417, <https://doi.org/10.5194/acp-20-9393-2020>, 2020.
- 755 Dai, T., Schutgens, N., Goto, D., Shi, G., and Nakajima, T.: Improvement of aerosol optical properties modeling over Eastern Asia with MODIS AOD assimilation in a global non-hydrostatic icosahedral aerosol transport model, *Environmental Pollution*, 195, 319–329, <https://doi.org/10.1016/j.envpol.2014.06.021>, 2014.
- 760 Descheemaeker, M., Plu, M., Marécal, V., Claeysman, M., Olivier, F., Aoun, Y., Blanc, P., Wald, L., Guth, J., Sič, B., Vidot, J., Piacentini, A., and Josse, B.: Monitoring aerosols over Europe: an assessment of the potential benefit of assimilating the VIS04 measurements from the future MTG/FCI geostationary imager, *Atmospheric Measurement Techniques*, 12, 1251–1275, <https://doi.org/10.5194/amt-12-1251-2019>, 2019.
- Diehl, T., Heil, A., Chin, M., Pan, X., Streets, D., Schultz, M., and Kinne, S.: Anthropogenic, biomass burning, and volcanic emissions of black carbon, organic carbon, and SO₂ from 1980 to 2010 for hindcast model experiments, *Atmospheric Chemistry and Physics Discussions*, 12, 24 895–24 954, <https://doi.org/10.5194/acpd-12-24895-2012>, 2012.
- 765 El Amraoui, L., Attié, J.-L., N., S., Claeysman, M., Peuch, V.-H., Warner, J., Ricaud, P., Cammas, J.-P., Piacentini, A., Josse, B., Cariolle, D., Massart, S., and Bencherif, H.: Midlatitude stratosphere - troposphere exchange as diagnosed by MLS O₃ and MOPITT CO assimilated fields, *Atmospheric Chemistry and Physics*, 10, 2175–2194, <https://doi.org/10.5194/acp-10-2175-2010>, 2010.
- 770 Emmons, L. K., Walters, S., Hess, P. G., Lamarque, J.-F., Pfister, G. G., Fillmore, D., Granier, C., Guenther, A., Kinnison, D., Laepple, T., Orlando, J., Tie, X., Tyndall, G., Wiedinmyer, C., Baughcum, S., and Kloster, S.: Description and evaluation of the Model for Ozone and Related chemical Tracers, version 4 (MOZART-4), *Geoscientific Model Development*, 3, 43–67, <https://doi.org/10.5194/gmd-3-43-2010>, 2010.
- 775 Feichter, J., Kjellström, E., Rodhe, H., Dentener, F., Lelieveld, J., and Roelofs, G.-J.: Simulation of the tropospheric sulfur cycle in a global climate model, *Atmospheric Environment*, 30, 1693–1707, [https://doi.org/10.1016/1352-2310\(95\)00394-0](https://doi.org/10.1016/1352-2310(95)00394-0), 1996.

- Feinberg, A., Sukhodolov, T., Luo, B.-P., Rozanov, E., Winkel, L. H. E., Peter, T., and A., S.: Improved tropospheric and stratospheric sulfur cycle in the aerosol–chemistry–climate model SOCOL-AERv2, *Geoscientific Model Development*, 12, 3863–3887, <https://doi.org/10.5194/gmd-12-3863-2019>, 2019.
- 780 Fioletov, V. E., McLinden, C. A., Krotkov, N., Yang, K., Loyola, D. G., Valks, P., Theys, N., Van Roozendaal, M., Nowlan, C. R., Chance, K., Liu, X., Lee, C., and Martin, R. V.: Application of OMI, SCIAMACHY, and GOME-2 satellite SO₂ retrievals for detection of large emission sources, *Journal of Geophysical Research: Atmospheres*, 118, 11 399–11 418, <https://doi.org/10.1002/jgrd.50826>, 2013.
- Fioletov, V. E., McLinden, C. A., Krotkov, N., Li, C., Joiner, J., Theys, N., Carn, S., and Moran, M. D.: A global catalogue of large SO₂ sources and emissions derived from the Ozone Monitoring Instrument, *Atmospheric Chemistry and Physics*, 16, 11 497–11 519, <https://doi.org/10.5194/acp-16-11497-2016>, 2016.
- 785 Fioletov, V. E., McLinden, C. A., Griffin, D., Theys, N., Loyola, D. G., Hedelt, P., Krotkov, N., and Li, C.: Anthropogenic and volcanic point source SO₂ emissions derived from TROPOMI on board Sentinel-5 Precursor: first results, *Atmospheric Chemistry and Physics*, 20, 5591–5607, <https://doi.org/10.5194/acp-20-5591-2020>, 2020.
- Fountoukis, C. and Nenes, A.: ISORROPIA II: a computationally efficient thermodynamic equilibrium model for K⁺ - Ca²⁺ - Mg²⁺ - NH₄⁺ - Na⁺ - SO₄²⁻ - NO₃⁻ - Cl⁻ - H₂O aerosols, *Atmospheric Chemistry and Physics*, 7, 4639–4659, <https://doi.org/10.5194/acp-7-4639-2007>, 2007.
- 790 Freitas, S. R., Longo, K. M., Alonso, M. F., Pirre, M., Marécal, V., Grell, G., Stockler, R., Mello, R. F., and Sanchez Gacita, M.: A pre-processor of trace gases and aerosols emission fields for regional and global atmospheric chemistry models, *Geoscientific Model Developments*, 4, 419–433, <https://doi.org/10.5194/gmdd-3-855-2010>, 2011.
- Gasso, S.: Satellite observations of the impact of weak volcanic activity on marine clouds, *Journal of Geophysical Research*, 113, <https://doi.org/10.1029/2007JD009106>, 2008.
- 795 Ge, C., Wang, J., Carn, S., Yang, K., Ginoux, P., and Krotkov, N.: Satellite-based global volcanic SO₂ emissions and sulfate direct radiative forcing during 2005–2012, *Journal of Geophysical research*, 121, 1–19, <https://doi.org/10.1002/2015JD023134>, 2016.
- Gondwe, M., Krol, M., Gieskes, W., Klaasen, W., and de Baar, H.: The contribution of ocean-leaving DMS to the global atmospheric burdens of DMS, MSA, SO₂ and NSS SO₄⁻, *Global Biogeochemical Cycles*, 17, 1056, <https://doi.org/10.1029/2002GB001937>, 2003a.
- 800 Gondwe, M., Krol, M., Gieskes, W., Klaasen, W., and de Baar, H.: Correction to "The contribution of ocean-leaving DMS to the global atmospheric burdens of DMS, MSA, SO₂ and NSS SO₄⁻", *Global Biogeochemical Cycles*, 17, 1106, <https://doi.org/10.1029/2003GB002153>, 2003b.
- Graf, H.-F., Feichter, J., and Langmann, B.: Volcanic sulfur emissions: Estimates of source strength and its contribution to the global sulfate distribution, *Journal of Geophysical Research*, 102, 10 727–10 728, <https://doi.org/10.1029/96JD03265>, 1997.
- 805 Graf, H.-F., Langmann, B., and Feichter, J.: The contribution of Earth degassing to the atmospheric sulfur budget, *Chemical Geology*, 147, 131–145, [https://doi.org/10.1016/S0009-2541\(97\)00177-0](https://doi.org/10.1016/S0009-2541(97)00177-0), 1998.
- Gunson, J. R., Spall, S. A., Anderson, T. R., Jones, A., Totterdell, I. J., and Woodage, M. J.: Climate sensitivity to ocean dimethylsulphide emissions, *Geophysical Research Letters*, 33, <https://doi.org/10.1029/2005GL024982>, 2006.
- Guth, J.: Modélisation des aérosols à l'aide du modèle de chimie-transport MOCAGE : application à la qualité de l'air dans le bassin méditerranéen, Ph.D. thesis, Université Toulouse III Paul Sabatier, 2015.
- 810 Guth, J., Josse, B., Marécal, V., Joly, M., and Hamer, P.: First implementation of secondary inorganic aerosols in the MOCAGE version R2.15.0 chemistry transport model, *Geoscientific Model Development*, 9, 137–160, <https://doi.org/10.5194/gmd-9-137-2016>, 2016.

- Guth, J., Marécal, V., Josse, B., Arteta, J., and Hamer, P.: Primary aerosols and secondary inorganic aerosol budget over the Mediterranean Basin during 2012 and 2013, *Atmospheric Chemistry and Physics*, 18, <https://doi.org/10.5194/acp-18-4911-2018>, 2018.
- 815 Halmer, M., Schmincke, H.-U., and Graf, H.-F.: The annual volcanic gas input into the atmosphere, in particular into the stratosphere: a global data set for the past 100 years, *Journal of Volcanology and Geothermal Research*, 115, 511–528, [https://doi.org/10.1016/S0377-0273\(01\)00318-3](https://doi.org/10.1016/S0377-0273(01)00318-3), 2002.
- He, H., Li, C., Loughner, C. P., Li, Z., Krotkov, N. A., Yang, K., Wang, L., Zheng, Y., Bao, X., Zhao, G., and Dickerson, R. R.: SO₂ over central China: Measurements, numerical simulations and the tropospheric sulfur budget, *Journal of Geophysical Research*, 117, <https://doi.org/10.1029/2011JD016473>, 2012.
- 820 Josse, B., Simon, P., and Peuch, V.: Radon global simulations with the multiscale chemistry and transport model MOCAGE, *Tellus B: Chemical and Physical Meteorology*, 56, 339–356, <https://doi.org/10.3402/tellusb.v56i4.16448>, 2004.
- Kaiser, J. W., Heil, A., Andreae, M., Benedetti, A., Chubarova, N., Jones, L., Morcrette, J.-J., Razinger, M., Schultz, M. G., Suttie, M., and van der Werf, G. R.: Biomass burning emissions estimated with a global fire assimilation system based on observed fire radiative power, *Biogeosciences*, 9, 527–554, <https://doi.org/10.5194/bg-9-527-2012>, 2012.
- 825 Kettle, A., Andreae, M. O., Amouroux, D., Andreae, T. W., Bates, T. S., Berresheim, H., Bingemer, H., Boniforti, R., Curran, M., DiTullio, G. R., Helas, G., Jones, G. B., Kiene, R. P., Leck, C., Levasseur, M., Malin, G., Maspero, M., Matrai, P., McTaggart, A. R., Mihalopoulos, N., Nguyen, B. C., Novo, A., Putaud, J. P., Rapsomanikis, S., Roberts, G., Schebeske, G., Sharma, S., Simó, R., Staubes, R., Turner, S., and Uher, G.: A global database of sea surface dimethylsulfide (DMS) measurements and a procedure to predict sea surface DMS as a function of latitude, longitude, and month, *Global Biogeochemical Cycles*, 13, 399–444, <https://doi.org/10.1029/1999GB900004>, 1999.
- 830 Koren, I., Remer, L. A., Kaufman, Y. J., Rudich, Y., and Martins, J. V.: On the twilight zone between clouds and aerosols, *Geophysical Research Letters*, 34, <https://doi.org/10.1029/2007GL029253>, 2007.
- Kremser, S., Thomason, L. W., von Hobe, M., Hermann, M., Deshler, T., Timmreck, C., Toohey, M., Stenke, A., Schwarz, J. P., Weigel, R., Fueglistaler, S., Prata, F. J., Vernier, J.-P., Schlager, H., Barnes, J. E., Antuña-Marrero, J.-C., Fairlie, D., Palm, M., Mahieu, E., Notholt, J., Rex, M., Bingen, C., Vanhellemont, F., Bourassa, A., Plane, J. M. C., Klocke, D., Carn, S. A., Clarisse, L., Trickl, T., Neely, R., James, A. D., Rieger, L., Wilson, J. C., and Meland, B.: Stratospheric aerosol—Observations, processes, and impact on climate, *Reviews of Geophysics*, 54, 278–335, <https://doi.org/10.1002/2015RG000511>, 2016.
- 835 Krotkov, N. A., McLinden, C. A., Li, C., Lamsal, L. N., Celarier, E. A., Marchenko, S. V., Swartz, W. H., Bucsele, E. J., Joiner, J., N., D. B., Boersma, F., Veefkind, P., Levelt, P. F., Fioletov, V. E., Dickerson, R. R., He, H., Lu, Z., and Streets, D.: Aura OMI observations of regional SO₂ and NO₂ pollution changes from 2005 to 2015, *Atmospheric Chemistry and Physics*, 16, 4605–4629, <https://doi.org/10.5194/acp-16-4605-2016>, 2016.
- 840 Krueger, A., Walter, L., Bhartia, P., Schnetzler, C., Krotkov, N., Sprod, I., and Bluth, G.: Volcanic sulfur dioxide measurements from the total ozone mapping spectrometer instruments, *Journal of Geophysical Research*, 100, 14 057–14 076, <https://doi.org/10.1029/95JD01222>, 1995.
- 845 Köpke, P., Hess, M., Schult, I., and Shettle, E.: Global Aerosol Data Set, <http://hdl.handle.net/10068/256361>, 1997.
- Lacressonnière, G., Peuch, V.-H., Vautard, R., Arteta, J., Déqué, M., Joly, M., Josse, B., Marécal, V., and Saint-Martin, D.: European air quality in the 2030s and 2050s: Impacts of global and regional emission trends and of climate change, *Atmospheric Environment*, 92, 348–358, <https://doi.org/10.1016/j.atmosenv.2014.04.033>, 2014.

- Lacressonnière, G., Foret, G., Beekmann, M., Siour, G., Engardt, M., Gauss, M., Watson, L., Andersson, C., Colette, A., Josse, B., Marécal, V., Nyiri, A., and Vautard, R.: Impacts of regional climate change on air quality projections and associated uncertainties, *Climatic Change*, 136, 309–324, <https://doi.org/10.1007/s10584-016-1619-z>, 2016.
- Lacressonnière, G., Watson, L., Gauss, M., Engardt, M., Andersson, C., Beekmann, M., Colette, A., Foret, G., Josse, B., Marécal, V., Nyiri, A., Siour, G., Sobolowski, S., and Vautard, R.: Particulate matter air pollution in Europe in a +2 C warming world, *Atmospheric Environment*, 154, 129–140, <https://doi.org/10.1016/j.atmosenv.2017.01.037>, 2017.
- Lamarque, J.-F., Bond, T. C., Eyring, V., Granier, C., Heil, A., Klimont, Z., Lee, D., Liousse, C., Mieville, A., Owen, B., Schultz, M. G., Shindell, D., Smith, S. J., Stehfest, E., Van Aardenne, J., Cooper, O. R., Kainuma, M., Mahowald, N., McConnell, J. R., Naik, V., Riahi, K., and van Vuuren, D. P.: Historical (1850–2000) gridded anthropogenic and biomass burning emissions of reactive gases and aerosols: methodology and application, *Atmospheric Chemistry and Physics*, 10, 7017–7039, <https://doi.org/10.5194/acp-10-7017-2010>, 2010.
- Lamarque, J.-F., Emmons, L. K., Hess, P. G., Kinnison, D. E., Tilmes, S., Vitt, F., Heald, C. L., Holland, E. A., Lauritzen, P. H., Neu, J., Orlando, J. J., Rasch, P. J., and Tyndall, G. K.: CAM-chem: description and evaluation of interactive atmospheric chemistry in the Community Earth System Model, *Geoscientific Model Development*, 5, 369–411, <https://doi.org/10.5194/gmd-5-369-2012>, 2012.
- Lamarque, J.-F., Shindell, D., Josse, B., Young, P., Cionni, I., Eyring, V., Bergmann, D., Cameron-Smith, P., Collins, W., Doherty, R., Dalsoren, S., Faluvegi, G., Folberth, G., Ghan, S., Horowitz, L., Lee, Y., MacKenzie, I., Nagashima, T., Naik, V., Plummer, D., Righi, M., Rumbold, S., Schulz, M., Skeie, R., Stevenson, D., Strode, S., Sudo, K., Szopa, S., Voulgarakis, A., and Zeng, G.: The Atmospheric Chemistry and Climate Model Intercomparison Project (ACCMIP): overview and description of models, simulations and climate diagnostics, *Geoscientific Model Development*, 6, 179–206, <https://doi.org/10.5194/gmd-6-179-2013>, 2013.
- Lefèvre, F., Brasseur, P., Folkins, I., Smith, A. K., and Simon, P.: Chemistry of the 1991–1992 stratospheric winter : Three-dimensional simulations, *Journal of Geophysical Research*, 99, 8183–8195, <https://doi.org/10.1029/93JD03476>, 1994.
- Li, C., Joiner, J., Krotkov, N., and Bhartia, P.: A fast and sensitive new satellite SO₂ retrieval algorithm based on principal component analysis: Application to the ozone monitoring instrument, *Geophysical Research Letters*, 40, 6314–6318, <https://doi.org/10.1002/2013GL058134>, 2013.
- Li, C., Krotkov, N. A., Leonard, P., and Joiner, J.: OMI/Aura Sulphur Dioxide (SO₂) Total Column 1-orbit L2 Swath 13x24 km V003, <https://doi.org/10.5067/Aura/OMI/DATA2022>, <https://doi.org/10.5067/Aura/OMI/DATA2022>, accessed [01/02/2020], 2020.
- Li, Z., Liu, Q., Lin, H.-C., Schwartz, C. S., and Lee, Y.-H., W. T.: Three-dimensional variational assimilation of MODIS aerosol optical depth: Implementation and application to a dust storm over East Asia, *Journal of Geophysical Research: Atmospheres*, 116, <https://doi.org/10.1029/2011JD016159>, 2011.
- Liu, X., Penner, J. E., and Herzog, M.: Global modeling of aerosol dynamics: Model description, evaluation, and interactions between sulfate and nonsulfate aerosols, *Journal of Geophysical Research*, 110, <https://doi.org/10.1029/2004JD005674>, 2005.
- Liu, X., Penner, J. E., Das, B., Bergmann, D., Rodriguez, J. M., Strahan, S., Wang, M., and Feng, Y.: Uncertainties in global aerosol simulations: Assessment using three meteorological data sets, *Journal of Geophysical Research*, 112, <https://doi.org/10.1029/2006JD008216>, 2007.
- Louis, J.-F.: A parametric model of vertical eddy fluxes in the atmosphere, *Boundary Layer Meteorology*, 17, 187–202, <https://doi.org/10.1007/BF00117978>, 1979.
- Madronich, S.: Photodissociation in the atmosphere: 1. Actinic flux and the effects of ground reflections and clouds, *Journal of Geophysical Research: Atmospheres*, 92, 9740–9752, <https://doi.org/10.1029/JD092iD08p09740>, 1987.

- Martet, M., Peuch, V., Laurent, B., Marticorena, B., and Bergametti, G.: Evaluation of long-range transport and deposition of desert dust with the CTM MOCAGE, *Tellus B: Chemical and Physical Meteorology*, 61, 449–463, <https://doi.org/10.1111/j.1600-0889.2008.00413.x>, 2009.
- 890 Marécal, V., Peuch, V.-H., Andersson, C., Andersson, S., Arteta, J., Beekmann, M., Benedictow, A., Bergström, R., Bessagnet, B., Cansado, A., Chéroux, F., Colette, A., Coman, A., Curier, R., Denier van der Gon, H., Drouin, A., Elbern, H., Emili, E., Engelen, R., Eskes, H., Foret, G., Friese, E., Gauss, M., Giannaros, C., Guth, J., Joly, M., Jaumouillé, E., Josse, B., Kadygrov, N., Kaiser, J., Krajsek, K., Kuenen, J., Kumar, U., Liora, N., Lopez, E., Malherbe, L., Martinez, I., Melas, D., Meleux, F., Menut, L., Moinat, P., Morales, T., Parmentier, J., Piacentini, A., Plu, M., Poupkou, A., Queguiner, S., Robertson, L., Rouïl, L., Schaap, M., Segers, A., Sofiev, M., Tarasson, L., Thomas, M., Timmermans, R., Valdebenito, A., van Velthoven, P., van Versendaal, R., Vira, J., and Ung, A.: A regional air quality forecasting system
895 over Europe: the MACC-II daily ensemble production, *Geoscientific Model Development*, 8, 2777–2813, <https://doi.org/10.5194/gmd-8-2777-2015>, 2015.
- Michou, M., Nabat, P., and Saint-Martin, D.: Development and basic evaluation of a prognostic aerosol scheme (v1) in the CNRM Climate Model CNRM-CM6, *Geoscientific Model Development*, 8, 501–531, <https://doi.org/10.5194/gmd-8-501-2015>, 2015.
- Michou, M., Nabat, P., Saint-Martin, D., Bock, J., Decharme, B., Mallet, M., Roehrig, R., Séférian, R., Sénési, S., and Voldoire, A.: Present-
900 Day and Historical Aerosol and Ozone Characteristics in CNRM CMIP6 Simulations, *Journal of Advances in Modeling Earth Systems*, 12, <https://doi.org/10.1029/2019MS001816>, 2019.
- Moffat, A. and Millan, M.: The application of optical correlation techniques to the remote sensing of SO₂ plumes using sky light, *Atmospheric Environment*, 5, 677–690, [https://doi.org/10.1016/0004-6981\(71\)90125-9](https://doi.org/10.1016/0004-6981(71)90125-9), 1971.
- Nenes, A., Pilinis, C., and Pandis, N.: ISORROPIA : A new thermodynamic equilibrium model for multiphase multicomponent inorganic
905 aerosols, *Aquatic Geochemistry*, 4, 123–152, <https://doi.org/10.1023/A:1009604003981>, 1998.
- Nowlan, C., Liu, X., Chance, K., Cai, Z., Kurosu, T., Lee, C., and Martin, R.: Retrieval of sulfur dioxide from the Global Ozone Monitoring Experiment 2 (GOME-2) using an optimal estimation approach: Algorithm and initial validation, *Journal of Geophysical Research*, 116, <https://doi.org/10.1029/2011JD015808>, 2011.
- Pham, M., Muller, J., Brasseur, G. P., Granier, C., and Megie, G.: A three-dimensional study of the tropospheric sulfur cycle, *Journal of
910 Geophysical Research*, 100, 26 061–26 092, <https://doi.org/10.1029/95JD02095>, 1995.
- Price, C., Penner, J., and Prather, M.: NO_x from lightning: 1. global distribution based on lightning physics, *Journal of Geophysical Research: Atmospheres*, 102, 5929–5941, <https://doi.org/10.1029/96JD03504>, 1997.
- Remer, L. A., Kleidman, R. G., Levy, R. C., Kaufman, Y. J., Tanré, D., Mattoo, S., Vanderlei Martins, J. V., Ichoku, C., Koren, I., Yu, H., and Holben, B. N.: Global aerosol climatology from the MODIS satellite sensors, *Journal of Geophysical Research*, 113,
915 <https://doi.org/10.1029/2007JD009661>, 2008.
- Richter, A., Wittrock, F., and Burrows, J. P.: SO₂ measurements with SCIAMACHY, in: European Space Agency Center for Earth Observation, Frascati, Italy, paper presented at Atmospheric Science Conference, 2006.
- Rix, M., Valks, P., Hao, N., Loyola, D., Schlager, H., Huntrieser, H., Flemming, J., Koehler, U., Schumann, U., and Inness, A.: Volcanic SO₂, BrO and plume height estimations using GOME-2 satellite measurements during the eruption of Eyjafjallajökull in May 2010, *Journal of
920 Geophysical Research*, 117, <https://doi.org/10.1029/2011JD016718>, 2012.
- Robock, A.: Volcanic eruptions and climate, *Reviews of Geophysics*, 38, 191–219, <https://doi.org/10.1029/1998RG000054>, 2000.
- Robock, A.: Correction to "Volcanic eruptions and climate", *Reviews of Geophysics*, 45, <https://doi.org/10.1029/2007RG000232>, 2007.

- Rouil, L., Honoré, C., Bessagnet, B., Malherbe, L., Meleux, F., Vautard, R., Beekmann, M., Flaud, J.-M., Dufour, A., Martin, D., Peuch, A., Peuch, V.-H., Elichegaray, C., Poisson, N., and Menut, L.: PREV' AIR: an operational forecasting and mapping system for air quality in Europe, *Bulletin of the American Meteorological Society*, 90, 73–84, <https://doi.org/10.1175/2008BAMS2390.1>, 2009.
- 925 Ruiz-Arias, J. A., Dudhia, J., Gueymard, C. A., and Pozo-Vázquez, D.: Assessment of the Level-3 MODIS daily aerosol optical depth in the context of surface solar radiation and numerical weather modeling, *Atmospheric Chemistry and Physics*, 13, 675–692, <https://doi.org/10.5194/acp-13-675-2013>, 2013.
- Savage, N. H., Agnew, P., Davis, L. S., Ordóñez, C., Thorpe, R., Johnson, C. E., O'Connor, F. M., and Dalvi, M.: Air quality modelling using the Met Office Unified Model (AQUA OS24-26): model description and initial evaluation, *Geoscientific Model Development*, 6, 353–372, <https://doi.org/10.5194/gmd-6-353-2013>, 2013.
- 930 Schaefer, S. J., Kerr, J. B., Millán, M. M., Realmuto, V. J., Krueger, A. J., Krotkov, N. A., Seftor, C., and Sprod, I. E.: Geophysicists Unite to Validate Volcanic SO₂ Measurements, *EOS, Transactions American Geophysical Union*, 78, 217–223, <https://doi.org/10.1029/97EO00144>, 2011.
- 935 Schenkeveld, V. M. E., Jaross, G., Marchenko, S., Haffner, D., Kleipool, Q. L., Rozemeijer, N. C., Veefkind, J. P., and Levelt, P. F.: In-flight performance of the Ozone Monitoring Instrument, *Atmospheric Measurement Techniques*, 10, 1957–1986, <https://doi.org/10.5194/amt-10-1957-2017>, 2017.
- Schmidt, A., Carslaw, K., Mann, G., Rap, A., Pringle, K., Spracklen, D., Wilson, M., and Forster, P.: Importance of tropospheric volcanic aerosol for indirect radiative forcing of climate, *Atmospheric Chemistry and Physics*, 12, 7321–7339, <https://doi.org/10.5194/acp-12-7339-2012>, 2012.
- 940 Schmidt, A., Leadbetter, S., Theys, N., Carboni, E., Witham, C. S., Stevenson, J. A., Birch, C. E., Thordarson, T., Turnock, S., Barsotti, S., Delaney, L., Feng, W., Grainger, R. G., Hort, M. C., Höskuldsson, A., Ialongo, I., Ilyinskaya, E., Jóhannsson, T., Kenny, P., Mather, T. A., Richards, N. A. D., and Shepherd, J.: Satellite detection, long-range transport, and air quality impacts of volcanic sulfur dioxide from the 2014–2015 flood lava eruption at Bárðarbunga (Iceland), *Journal of Geophysical Research*, 120, 9739–9757, <https://doi.org/10.1002/2015JD023638>, 2015.
- 945 Seftor, C., Hsu, N., Herman, J., Bhartia, P., Torres, O., Rose, W., Schneider, D., and Krotkov, N.: Detection of volcanic ash clouds from Nimbus 7/total ozone mapping spectrometer, *Journal of Geophysical Research*, 102, 16 749–16 759, <https://doi.org/10.1029/97JD00925>, 1997.
- Seigneur, C., Pun, B., Pai, P., Louis, J.-F., Solomon, P., Emery, C., Morris, R., Zahniser, M., Worsnop, D., Koutrakis, P., White, W., and Tombach, I.: Guidance for the performance evaluation of three-dimensional air quality modeling systems for particulate matter and visibility, *Journal of the Air and Waste Management Association*, 50, 588–599, <https://doi.org/10.1080/10473289.2000.10464036>, 2000.
- Sellitto, P., Zanellet, C., di Sarra, A., Salerno, G., Tapparo, A., Meloni, D., Pace, G., Caltabiano, T., Briole, P., and Legrasa, B.: The impact of Mount Etna sulfur emissions on the atmospheric composition and aerosol properties in the central Mediterranean: A statistical analysis over the period 2000–2013 based on observations and Lagrangian modelling, *Atmospheric Environment*, 148, 77–88, <https://doi.org/10.1016/j.atmosenv.2016.10.032>, 2017.
- 955 Shaffrey, L. C., Stevens, I., Norton, W. A., Roberts, M. J., Vidale, P. L., Harle, J. D., Jarrar, A., Stevens, D. P., Woodage, M. J., Demory, M. E., Donners, J., Clark, D. B., Clayton, A., Cole, J. W., Wilson, S. S., Connolley, W. M., Davies, T. M., Iwi, A. M., Johns, T. C., King, J. C., New, A. L., Slingo, J. M., Steenman-Clark, L., and Martin, G. M.: U.K. HiGEM; The New U.K. High-Resolution Global Environment Model - Model Description and Basic Evaluation, *Journal of Climate*, 22, 1861–1896, <https://doi.org/10.1175/2008JCLI2508.1>, 2009.

- 960 Sheng, J.-X., Weisenstein, D. K., Luo, B. P., Rozanov, E., Stenke, A., Anet, J., Bingemer, H., and Peter, T.: Global atmospheric sulfur budget under volcanically quiescent conditions: Aerosol-chemistry-climate model predictions and validation, *Journal of Geophysical Research: Atmospheres*, 120, 256–276, <https://doi.org/10.1002/2014JD021985>, 2015.
- Sindelarova, K., Granier, C., Bouarar, I., Guenther, A., Tilmes, S., Stavrou, T., Müller, J.-F., Kuhn, U., Stefani, P., and Knorr, W.: Global dataset of biogenic VOC emissions calculated by the MEGAN model over the last 30 years, *Atmospheric Chemistry and Physics*, 14, 9317–9341, <https://doi.org/10.5194/acp-14-9317-2014>, 2014.
- 965 Sič, B., El Amraoui, L., Marécal, V., Josse, B., Arteta, J., Guth, J., Joly, M., and Hamer, P.: Modelling of primary aerosols in the chemical transport model MOCAGE: development and evaluation of aerosol physical parametrizations, *Geoscientific Model Development*, 8, 381–408, <https://doi.org/10.5194/gmd-8-381-2015>, 2015.
- Smith, S., Pitcher, H., and Wigley, T.: Global and regional anthropogenic sulfur dioxide emissions, *Global and Planetary Change*, 29, 99–119, [https://doi.org/10.1016/S0921-8181\(00\)00057-6](https://doi.org/10.1016/S0921-8181(00)00057-6), 2001.
- 970 Stevenson, D. S., Johnson, C. E., Collins, W. J., and Derwent, R.: The tropospheric sulphur cycle and the role of volcanic SO₂, in: *Volcanic Degassing*, edited by Oppenheimer, C., Pyle, D., and Barclay, J., vol. 213, pp. 295–305, Geological Society, London, special publications edn., 2003.
- Stockwell, W. R., Kirchner, F., Kuhn, M., and Seefeld, S.: A new mechanism for regional atmospheric chemistry modeling, *Journal of Geophysical Research*, 102, 25 847–25 879, <https://doi.org/10.1029/97JD00849>, 1997.
- 975 Stuefer, M., Freitas, S. R., Grell, G., Webley, P., Peckham, S., McKeen, S. A., and Egan, S. D.: Inclusion of ash and SO₂ emissions from volcanic eruptions in WRF-Chem: development and some applications, *Geoscientific Model Development*, 6, 457–468, <https://doi.org/10.5194/gmd-6-457-2013>, 2013.
- Sun, W., Shao, M., Granier, C., Liu, Y., and Zheng, J. Y.: Long-term trends of anthropogenic SO₂, NO_x, CO, and NMVOCs emissions in China, *Earth's Future*, 6, 1112–1133, <https://doi.org/10.1029/2018EF000822>, 2018.
- 980 Takemura, T.: Distributions and climate effects of atmospheric aerosols from the preindustrial era to 2100 along Representative Concentration Pathways (RCPs) simulated using the global aerosol model SPRINTARS, *Atmospheric Chemistry and Physics*, 12, 11 555–11 572, <https://doi.org/10.5194/acp-12-11555-2012>, 2012.
- Taylor, I., Preston, J., Carboni, E., Mather, T. A., Grainger, R. G., Theys, N., Hidalgo, S., and McComick Kilbride, B.: Exploring the Utility of IASI for Monitoring Volcanic SO₂ Emissions, *Journal of Geophysical Research: Atmospheres*, 123, 5588–5606, <https://doi.org/10.1002/2017JD027109>, 2018.
- 985 Teyssèdre, H., Michou, M., Clark, H., Josse, B., Karcher, F., Olivieri, D., Peuch, V.-H., Saint-Martin, D., Cariolle, D., Attié, J.-L., Nédélec, P., Ricaud, P., Thouret, V., Van der A, R., Volz-Thomas, A., and Chéroux, F.: A new tropospheric and stratospheric Chemistry and Transport Model MOCAGE-Climat for multi-year studies: evaluation of the present-day climatology and sensitivity to surface processes, *Atmospheric Chemistry and Physics*, 7, 5815–5860, <https://doi.org/10.5194/acp-7-5815-2007>, 2007.
- 990 Theys, N., Hedelt, P., De Smedt, I., Lerot, C., Yu, H., Vlietinck, J., Pedernana, M., Arellano, S., Galle, B., Fernandez, D., Carlito, C. J. M., Barrington, C., Taisne, B., Delgado-Granados, H., Loyola, D., and Van Roozendaal, M.: Global monitoring of volcanic SO₂ degassing with unprecedented resolution from TROPOMI onboard Sentinel-5 Precursor, *Scientific Reports*, 9, 2643, <https://doi.org/10.1038/s41598-019-39279-y>, 2019.
- 995 Thomas, H., Watson, M., Carn, S.A. Prata, A., and Realmuto, V.: A comparison of AIRS, MODIS and OMI sulphur dioxide retrievals in volcanic clouds, *Geomatics, Natural Hazards and Risk*, 2, 217–232, <https://doi.org/10.1080/19475705.2011.564212>, 2011.

- Torres, O., Bhartia, P., Herman, J., Ahmad, Z., and Gleason, J.: Derivation of aerosol properties from satellite measurements of backscattered ultraviolet radiation: Theoretical basis, *Journal of Geophysical Research*, 103, 17 099–17 110, <https://doi.org/10.1029/98JD00900>, 1998a.
- 1000 Torres, O., Bhartia, P., Herman, J., Ahmad, Z., and Gleason, J.: Correction to "Derivation of aerosol properties from satellite measurements of backscattered ultraviolet radiation: Theoretical basis", *Journal of Geophysical Research*, 103, 23 321, <https://doi.org/10.1029/98JD02709>, 1998b.
- Walters, D. N., Williams, K. D., Boutle, I. A., Bushell, A., Edwards, J. M., Field, P. R., Lock, A. P., Morcrette, C. J., Stratton, R. A., Wilkinson, J. M., Willett, M. R., Bellouin, N., Bodas-Salcedo, A., Brooks, M. E., Copsey, D., Earnshaw, P. D., Hardiman, S. C., Harris, C. M., Levine, R. C., MacLachlan, C., Manners, J. C., Martin, G. M., Milton, S. F., Palmer, M. D., Roberts, M. J., Rodriguez, J. M., 1005 Tennant, W. J., and Vidale, P. L.: The Met Office Unified Model Global Atmosphere 4.0 and JULES Global Land 4.0 configurations, *Geoscientific Model Development*, 7, 361–386, <https://doi.org/10.5194/gmd-7-361-2014>, 2014.
- Wang, Y. and Wang, J.: Tropospheric SO₂ and NO₂ in 2012–2018: Contrasting views of two sensors (OMI and OMPS) from space, *Atmospheric environment*, 223, <https://doi.org/10.1016/j.atmosenv.2019.117214>, 2020.
- Wang, Y., Beirle, S., Lampel, J., Koukouli, M., De Smedt, I., Theys, N., Li, A., Wu, D., Xie, P., Liu, C., Van Roozendael, M., Stavrakou, T., 1010 Müller, J.-F., and Wagner, T.: Validation of OMI, GOME-2A and GOME-2B tropospheric NO₂, SO₂ and HCHO products using MAX-DOAS observations from 2011 to 2014 in Wuxi, China: investigation of the effects of priori profiles and aerosols on the satellite products, *Atmospheric Chemistry and Physics*, 17, 5007–5033, <https://doi.org/10.5194/acp-17-5007-2017>, 2017.
- Williams-Jones, G., Stix, J., and Nadeau, P.: Using the COSPEC in the Field, vol. 1 of *The COSPEC Cookbook: Making SO₂ Measurements at Active Volcanoes*, chap. 3, pp. 63–119, IAVCEI, Methods in Volcanology, 2008.
- 1015 Williamson, D. L. and Rasch, P. J.: Two dimensional semi-lagrangian transport with shape-preserving interpolation, *Monthly Weather Review*, 117, 102–129, [https://doi.org/10.1175/1520-0493\(1989\)117<0102:TDSLWTW>2.0.CO;2](https://doi.org/10.1175/1520-0493(1989)117<0102:TDSLWTW>2.0.CO;2), 1989.
- Wiscombe, W. J.: Improved Mie scattering algorithms, *Applied Optics*, 19, 1505–1509, <https://doi.org/10.1364/AO.19.001505>, 1980.
- Yang, K., Krotkov, N., Krueger, A., Carn, S., and Bhartia, P.K. Levelt, P.: Improving retrieval of volcanic sulfur dioxide from backscattered UV satellite observations, *Geophysical Research Letters*, 36, <https://doi.org/10.1029/2008GL036036>, 2009.
- 1020 Yang, K., Liu, X., Bhartia, P., Krotkov, N., Carn, S., Hughes, E., Krueger, A., Spurr, R. J., and Trahan, S.: Direct retrieval of sulfur dioxide amount and altitude from spaceborne hyperspectral UV measurements: Theory and application, *Journal of Geophysical Research*, 115, <https://doi.org/10.1029/2010JD013982>, 2010.
- Yang, K., Dickerson, R., Carn, S., Ge, C., and Wang, J.: First observations of SO₂ from the satellite Suomi NPP OMPS: Widespread air pollution events over China, *Geophysical Research Letters*, 40, 4957–4962, <https://doi.org/10.1002/grl.50952>, 2013.
- 1025 Zhang, J., Reid, J. S., and Holben, B. N.: An analysis of potential cloud artifacts in MODIS over ocean aerosol optical thickness products, *Geophysical Research Letters*, 32, <https://doi.org/10.1029/2005GL023254>, 2005.